T.C.
IŞIK UNIVERSTIY
SCHOOL OF GRADUATE STUDIES

MASTER THESIS
DEPARTMENT OF ELECTRICAL AND ELECTRONICS ENGINEERING
ELECTRONICS PROGRAM

Zeynep ARLI

PERFORMANCE ANALYSIS OF ONE-LAYER RSMA IN INDOOR MULTI-USER VLC

SUPERVISOR

Prof. Dr. Onur KAYA

İSTANBUL, September 2025

T.C.
IŞIK UNIVERSITY
SCHOOL OF GRADUATE STUDIES

MASTER THESIS
DEPARTMENT OF ELECTRICAL AND ELECTRONICS ENGINEERING
ELECTRONICS PROGRAM

Zeynep ARLI

(22ELEC5003)

PERFORMANCE ANALYSIS OF ONE-LAYER RSMA IN INDOOR MULTI-USER VLC

SUPERVISOR

Prof. Dr. Onur KAYA

İSTANBUL, September 2025

T.C.
IŞIK UNIVERSITY
SCHOOL OF GRADUATE STUDIES

MASTER THESIS
DEPARTMENT OF ELECTRICAL AND ELECTRONICS ENGINEERING
ELECTRONICS ENGINEERING PROGRAM

Zeynep ARLI
(22ELEC5003)

PERFORMANCE ANALYSIS OF ONE-LAYER RSMA IN INDOOR MULTI-USER VLC

Date: 30 / 09 / 2025

Thesis Supervisor: Prof. Dr. Onur KAYA / Işık University

Jury Members:

Asst. Prof. Dr. Farshad MIRAMIRKHANI / Işık University

Asst. Prof. Dr. Çağatay EDEMEN / Özyeğin University

İSTANBUL, September 2025

ÖZET

İÇ ORTAM ÇOK KULLANICILI VLC SİSTEMLERDE TEK KATMANLI RSMA PERFORMANS ANALİZİ

Görünür Işık Haberleşmesi (VLC), özellikle yüksek kapasiteli iç mekân ağları için geleneksel radyo-frekansı (RF) teknolojilerine güçlü bir tamamlayıcı olarak öne çıkmaktadır. Ancak, iç mekânlarda kullanıcı ve aydınlatıcı yoğunluğunun artması, önemli seviyede girişim ve kaynak yönetimi sorunları ortaya çıkarmaktadır. Oran-Bölmeli Çoklu Erişim (RSMA), girişimi etkin bir şekilde yönetme ve spektral verimliliği artırma potansiyeline sahip, yeni nesil bir çoklu erişim yöntemi olarak öne çıkmasına rağmen, gerçekçi VLC senaryolarındaki performansı büyük ölçüde araştırılmamıştır.

Bu tezde, gerçek donanım kısıtları altında, bir katmanlı RSMA'nın aşağı yönlü çok kullanıcılı MISO-VLC sistemlerindeki uygulanabilirliği ve performansı incelenmiştir. Fiziksel olarak doğru bir Lambertian doğrusal görüş (LOS) kanal modeli kullanılmış; LED akımı doğrusalığı ve aydınlatma gereksinimleri açıkça gözetilmiştir. Ortak önişlemci ve güç tahsisi problemi sayısal olarak optimize edilerek çözülmüş ve iki temel simülasyon çerçevesi oluşturulmuştur: (i) Farklı iletim güçleri ve kullanıcı yükleri altında RSMA ve güç-bölmeli NOMA (PD-NOMA) yöntemlerinin karşılaştırıldığı rastgele kullanıcı yerleşimi senaryosu; (ii) Kullanıcı konumlarının spektral verimlilik üzerindeki etkisinin haritalandığı mekânsal duyarlılık analizi.

Kapsamlı simülasyon sonuçları, RSMA'nın tüm test edilen kullanıcı yoğunlukları ve güç seviyelerinde PD-NOMA'ya kıyasla tutarlı şekilde üstün performans gösterdiğini ortaya koymaktadır. Düşük optik güç seviyelerinde RSMA, iki kullanıcı için %50'ye, yedi kullanıcı için ise \%300'ün üzerine çıkan göreli spektral verimlilik artışları sağlamaktadır; yüksek güçte ise özellikle yoğun kullanıcı senaryolarında bu iyileşmeler devam etmektedir. Ayrıntılı analizler, optik iletim gücü, kullanıcı yoğunluğu, mekânsal dağılım ve optik

donanım parametrelerinin sistem performansı üzerindeki etkilerini ortaya koymuştur. Mekânsal ısı haritası analizleri ise, gerçekçi VLC kurulumlarında kullanıcı yerleşimi ve aydınlatıcı geometrisinin önemini vurgulamaktadır.

Bu bulgular, RSMA'nın gelecek nesil iç mekân VLC sistemleri için esnek ve etkin bir çoklu erişim stratejisi olduğunu ve gerçekçi kısıtlar altında önemli kazançlar sağladığını doğrulamaktadır. Gelecek çalışmalar, kanal belirsizliği, görüş dışı (NLOS) koşullar, deneysel doğrulama ve uyarlanabilir kaynak yönetimi için makine öğrenmesi entegrasyonu gibi başlıkları ele almalıdır.

Anahtar Kelimeler: Görünür Işık Haberleşmesi (VLC), Oran Bölmeli Çoklu Erişim (RSMA), Çok Kullanıcılı MISO, Işın Şekillendirme Optimizasyonu, Girişim Yönetimi

ABSTRACT

PERFORMANCE ANALYSIS OF ONE-LAYER RSMA IN INDOOR MULTI-USER VLC

Visible Light Communication (VLC) has emerged as a promising complement to traditional radio-frequency (RF) wireless technologies, particularly for high-capacity indoor networks. However, the dense deployment of users and luminaries in indoor environments introduces significant interference and resource management challenges. Rate-Splitting Multiple Access (RSMA) has recently been advocated as a robust multiple access paradigm capable of managing interference and enhancing spectral efficiency, yet its potential in realistic VLC scenarios remains underexplored.

This thesis investigates the applicability and performance of one-layer RSMA in downlink multi-user MISO VLC systems under practical hardware constraints. A physically accurate Lambertian line-of-sight (LOS) channel model is adopted, explicitly considering LED current linearity and illumination requirements. The joint precoder and power allocation problem is formulated and solved using numerical optimization, with two simulation frameworks: (i) a random user placement configuration benchmarking RSMA against power-domain NOMA (PD-NOMA) under varying transmit powers and user loads, and (ii) a spatial sensitivity analysis mapping spectral efficiency with respect to user locations.

Comprehensive simulation results demonstrate that RSMA consistently outperforms PD-NOMA across all evaluated user densities and power budgets. At low optical power, RSMA yields relative spectral efficiency gains up to 50\% for two users and over 300% for seven users; at higher power, substantial improvements persist, especially for denser deployments. Detailed analyses reveal the impact of optical transmit power, user density, spatial distribution, and optical hardware parameters on system performance. Spatial heatmap analyses

further highlight the significance of user placement and luminaire geometry in practical VLC deployments.

The findings confirm RSMA as a flexible and effective multiple access strategy for next-generation indoor VLC systems, with substantial gains under realistic constraints. Future work should address channel uncertainty, non-line-of-sight conditions, experimental validation, and the integration of machine learning for adaptive resource management.

Keywords: Visible Light Communication (VLC), Rate-Splitting Multiple Access (RSMA), Multi-User MISO, Precoding Optimization, Interference Management

ACKNOWLEDGEMENT

First and foremost, I would like to express my deepest gratitude to my supervisor, Prof. Dr. Onur Kaya. His intellectual guidance, scientific rigor, and unwavering support have profoundly shaped my academic journey. Since my undergraduate years, his presence has been a continuous source of inspiration, and the impact of his mentorship will remain with me throughout my academic life.

I would also like to extend my heartfelt thanks to Asst. Prof. Dr. Farshad Miramirkhani for his valuable insights and encouragement throughout my work in this field. His support has been a constant since my early exposure to communications field and has meaningfully contributed to my growth.

I am grateful to my colleagues, Elifcan Zengin Şatıroğlu and Ali Murat Değirmenci, and my professor Dr. Ebru Gürsu Çimen for their endless support in my graduate studies.

Finally, I wish to thank my family and friends, whose patience, understanding, and belief in me gave me the strength to carry on. Their presence has been the foundation behind every success.

Zeynep ARLI

This thesis was supported by TÜBİTAK 1004 project entitled "Sürdürülebilir Kentler İçin İleri Teknolojiler Platformu", under the grant 22AG042.

To my beloved parents, Ayşe and Fatih….

TABLE OF CONTENTS

LIST OF FIGURES

LIST OF TABLES

ABBREVIATIONS LIST

1-RSMA: One-Layer Rate-Splitting Multiple Access

CSIT: Channel State Information at the Transmitter

FOV: Field of View

IM/DD: Intensity-Modulation Direct-Detection

IoT: Internet of Things

LED: Light Emitting Diode

LOS: Line-of-Sight

MIMO: Multiple-Input Multiple-Output

MISO: Multiple-Input Single-Output

MMR: Maximize the Minimum Rate

MMSE: Minimum Mean Square Error

MRT: Maximum Ratio Transfer

MU-LP: Multi-User Linear-Precoding

MU-MISO: Multi-User MISO

NOMA: Non-Orthogonal Multiple Access

OFDMA: Orthogonal Frequency-Division Multiple Access

OMA: Orthogonal Multiple Access

PD: Photo Diode

PD-NOMA: Power-Domain NOMA

RF: Radio Frequency

RIS: Reconfigurable Intelligent Surfaces

RSMA: Rate-Splitting Multiple Access

SC: Superposition Coding

SDMA: Space-Division Multiple Access

SE: Spectral Efficieny

SIC: Successive Interference Cancellation

SINR: Signal-to-Interference-plus-Noise Ratio

SVD: Singular Value Decomposition

TDMA: Time-Division Multiple Access

UWOC: Underwater Wireless Optical Communication

VLC: Visible Light Communication

ZF: Zero-Forcing

CHAPTER 1

1. INTRODUCTION

The exponential growth in global data demand has placed increasing pressure on conventional radio-frequency (RF) systems, which now struggle to satisfy the throughput, latency and security expectations of next-generation wireless applications. In dense indoor environments, propelled by Internet-of-Things (IoT) sensors, immersive reality services and ultra-high-definition streaming, spectral congestion and electromagnetic-compatibility constraints become particularly acute (Cisco, 2019; Soderi & De Nicola, 2022). These limitations have accelerated interest in alternative, spectrum-rich technologies that can coexist with established RF infrastructure without inducing further interference.

Visible-Light Communication (VLC) has therefore emerged as a compelling complement to RF. By exploiting the unlicensed 380–780 nm band and using light-emitting diodes (LEDs) as dual-purpose luminaries and transmitters, VLC inherits high modulation bandwidth, natural confinement to line-of-sight (LOS) links, and immunity to RF interference, all of which suit the stringent security and capacity demands of indoor networks that will underpin 6G services (Miramirkhani & Uysal, 2015). Nevertheless, as VLC evolves from point-to-point demonstrations to multi-user deployments, the challenges of user separation and interference management intensify (S. Naser et al., 2022). Because LED footprints often overlap and photodiode (PD) fields-of-view are directional, strong inter-user interference arises even in modest-size rooms. Traditional orthogonal schemes such as Time-Division Multiple Access (TDMA) or Orthogonal Frequency-Division Multiple Access (OFDMA) fail to exploit the full optical spectrum in these settings, while power-domain Non-Orthogonal Multiple Access (NOMA), though more flexible, is sensitive to LED non-linearity and user-channel asymmetry (Mohsan et al., 2023).

Rate-Splitting Multiple Access (RSMA) has recently been advocated as a unifying multiple-access paradigm that generalises both Space-Division Multiple Access (SDMA) and NOMA by superimposing a common message on user-specific private streams (Mao et al., 2022). Although RSMA has delivered robust gains in RF networks, its potential within VLC remains largely unexplored, especially when realistic optical channel models and hardware limits are taken into account (S. Naser et al., 2020). This thesis therefore investigates whether a one-layer RSMA strategy can enhance spectral efficiency in dense, hardware-constrained VLC deployments.

Concretely, we develop a downlink multi-user multiple-input single-output (MU-MISO) VLC system in which two ceiling-mounted LED arrays serve multiple PD-equipped users. A Lambertian channel model captures optical propagation, and the design explicitly observes LED current linearity, illumination requirements, and total transmit-power constraints. Building on this model, we cast the joint precoder–power-allocation problem and solve it using MATLAB's `fmincon` with the interior-point algorithm. Two complementary simulation structures are considered: one focuses on average spectral efficiency (SE) under varying user densities and power budgets, while the other explores how SE varies spatially with user positioning. Across both cases, SE is adopted as the primary performance metric. In the first structure, RSMA performance is also benchmarked against power-domain NOMA (PD-NOMA) to contextualize the results.

To explore the performance of RSMA under realistic indoor geometries, two distinct simulation methodologies are employed. In the first and main simulation framework, all users are randomly placed across the entire room area, reflecting practical deployments and allowing varying levels of inter-user channel correlation. This configuration is used to benchmark the spectral efficiency of RSMA against PD-NOMA under different transmit-power levels and user counts. As a complementary analysis, a spatial sensitivity study is conducted by fixing one user and sweeping a second user's position across a dense floor grid. Three distinct configurations are examined depending on the

location of the fixed user—near a room edge, directly under one LED, or centered between the two transmitters—enabling a detailed visualization of how spatial geometry affects RSMA performance.

Altogether, the thesis (i) puts forward a *comprehensive*, complexity-aware RSMA framework tailored to indoor optical wireless channels, (ii) demonstrates measurable spectral efficiency gains over baseline schemes in realistic conditions, and (iii) extracts design guidelines for both uniform and geometry-aware deployments. The spatial heat-map analysis further enriches this understanding by offering intuitive visual representations of throughput sensitivity to user position.

The remainder of this thesis is organized as follows. **Chapter 2** surveys the state-of-the-art SDMA, NOMA, and RSMA strategies in VLC, compares them, and identifies specific research gaps that motivate the present work. **Chapter 3** describes the physical set-up and channel model of the multi-user VLC system, detailing LED optics, PD characteristics, and the constraints imposed by illumination and device non-linearities. **Chapter 4** formulates the joint precoder–power-allocation problem and explains how it is solved using MATLAB's `fmincon` interior-point routine; the chapter also outlines the simulation workflow and the two user-placement configurations in detail. Finally, **Chapter 5** presents and analyzes the numerical results, and discusses implications for spectral efficiency and system design.

CHAPTER 2

2. LITERATURE REVIEW

2.1 VISIBLE LIGHT COMMUNICATION

VLC has emerged as a promising wireless communication technology that leverages the visible light spectrum (380-750 nm, Figure 2.1) for high-speed data transmission. Unlike conventional RF systems that operate in an already congested and regulated frequency space, VLC exploits a vast, license-free spectrum that is largely underutilized. This enables VLC to serve as a complementary or even alternative solution to RF systems, particularly in indoor environments where secure and interference-free communication is critical (Jovicic et al., 2013).

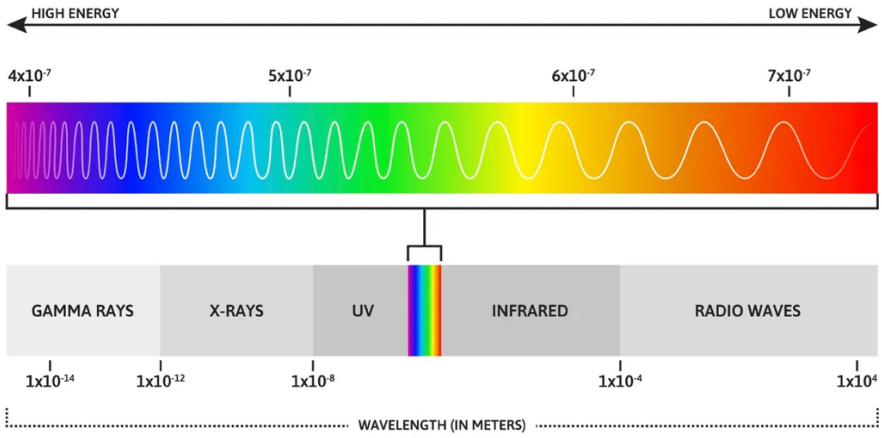

Figure 2.1: Visible Light Communication (Lucas, 2022).

In VLC systems, data transmission is achieved through rapid modulation of LEDs, which simultaneously provide illumination and serve as optical transmitters. On the receiving end, PDs are used to detect variations in light intensity, enabling high-speed data decoding through intensity modulation and

direct detection (IM/DD) techniques. Because visible light cannot penetrate opaque objects like walls, VLC inherently offers a high degree of spatial confinement and security, making it especially suitable for applications with stringent privacy requirements.

The dominant propagation condition in indoor VLC is typically LOS, as non-LOS components introduce severe attenuation and additional channel complexity. A Lambertian emission model is widely adopted to represent the angular radiation profile of LEDs (Pathak et al., 2015). In this model, the optical intensity decreases with the cosine of the irradiance angle, forming a cone-shaped illumination pattern (see: Figure 3.2). System-level parameters, such as the half-power semi-angle ($\Phi_{1/2}$), the field-of-view (FOV) of the receiver, and the vertical LED–PD separation, govern the coverage area and influence both signal strength and spatial reuse (system parameters are summarized in Table 4.1).

VLC systems offer several compelling advantages over traditional wireless technologies, including immunity to electromagnetic interference, access to unregulated bandwidth, and energy-efficient integration with existing lighting infrastructure (Mohsan et al., 2023). Moreover, due to their inherent spatial confinement, VLC links enhance physical-layer security, making them particularly attractive for applications involving short-range, high-data-rate communication (Maraqa et al., 2025).

This thesis investigates a downlink indoor VLC system employing multiple ceiling-mounted LED transmitters and multiple single-PD users. The overlapping LED beams lead to interference-dense regions, thereby necessitating efficient interference management techniques. RSMA is considered as a candidate strategy to address this challenge. A realistic Lambertian LOS model is adopted to characterize the optical channel and guide the optimization of precoding and power allocation strategies in subsequent chapters.

2.2 MULTI-USER TRANSMISSION STRATEGIES FOR VISIBLE LIGHT COMMUNICATION

2.2.1 Space-Division Multiple Access (SDMA)

SDMA exploits spatial multiplexing to serve several users in parallel. In an indoor VLC network the transmit array consists of multiple ceiling-mounted LEDs, while each receiver carries a single PD; the resulting channel is therefore MU-MISO. Linear multi-user precoding (MU-LP) such as zero-forcing (ZF), singular-value-decomposition (SVD) or minimum-mean-square-error (MMSE) processing is applied at the transmitter so that

$$y_k = \boldsymbol{h}_k^T \boldsymbol{W}\boldsymbol{x} + n_k, \qquad \boldsymbol{h}_i^T \boldsymbol{w}_j \approx 0 \; \forall \, i! \neq !\, j, \tag{2.1}$$

where $h_k \in \mathbb{R}^{N_t}$ denotes the Lambertian channel from the N_t LEDs to user k and $W = [w_1 \; \ldots \; w_K]$ is the MU-LP matrix. Because all interference is forced into the null space, no successive-interference-cancellation (SIC) is needed at the receiver (S. Naser et al., 2022), a desirable property for cost-sensitive IoT terminals. Figure 2.2 illustrates a representative SDMA-based downlink VLC architecture.

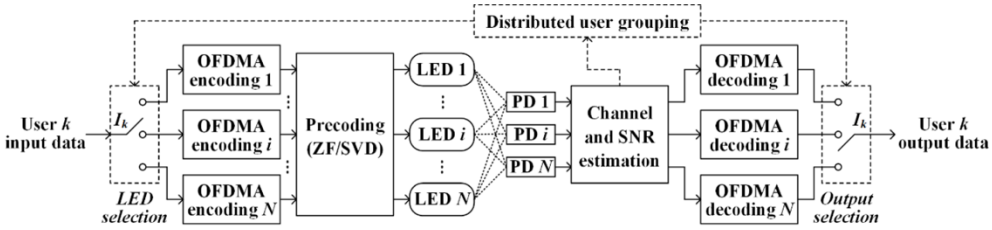

Figure 1.2: Block diagram of an SDMA-based VLC downlink system with precoding and distributed user grouping (Zhang et al., 2021).

n VLC, however, the practicality of SDMA is tightly linked to accurate channel-state information at the transmitter (CSIT) and to the ratio between active LEDs and addressed users. Indoor channels are quasi-static but measurement overhead and LED ageing still introduce CSIT errors; even a 3 dB

mismatch can collapse the spatial orthogonality assumed by ZF or SVD (Mao et al., 2018). Moreover, when the user count exceeds the LED count, as is common in multi-desk office layouts, orthogonal spatial beams cannot be formed and SDMA becomes infeasible (Qiu et al., 2025). Finally, dense LED panels demand per-element dimming control; if several LEDs must be switched off to maintain $\boldsymbol{h}_i^T \boldsymbol{w}_j = 0$, overall illumination may fall below building-code thresholds.

2.2.2 Power-Domain Non-Orthogonal Multiple Access (PD-NOMA)

PD-NOMA allows multiple users to simultaneously share the same spectral resources by superimposing their signals at different power levels. In VLC systems, this multiplexing is typically realized through IM/DD, with each PD receiving a linear combination of multiple user signals. The transmitter employs superposition coding (SC), while users employ SIC to decode their intended messages (Figure 2.3).

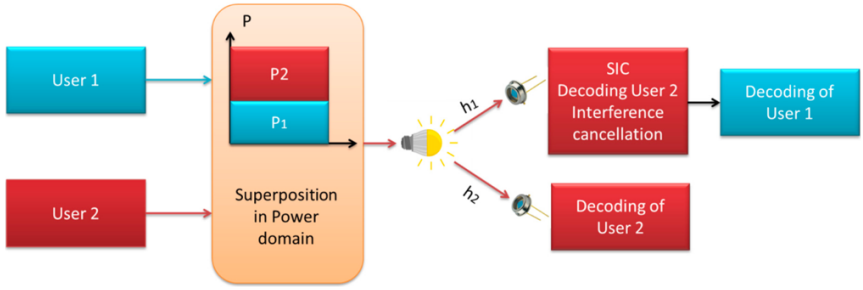

Figure 2.2: Architecture of a two-user downlink NOMA system in VLC (Mohsan et al., 2023).

In PD-NOMA, power levels are allocated inversely to the channel strengths: users with weaker channel gains are assigned more power to facilitate their detection at early stages of SIC. The key enabler here is the deterministic and largely time-invariant nature of the VLC channel, which allows accurate sorting of users based on LOS gain. Unlike RF-based NOMA, channel estimation in VLC can often rely on direct path geometry, making real-time power allocation more feasible (Marshoud et al., 2016).

A typical PD-NOMA precoding strategy adopts maximum ratio transmission (MRT), where each user's beamforming vector is aligned with its own channel. However, due to hardware constraints such as LED non-linearity and limited current headroom, power normalization must be carefully enforced When this is combined with sorted power allocation and SIC decoding, the achievable SE depends strongly on the disparity between user channels. Specifically, channel norm proximity reduces power allocation diversity and degrades SIC performance due to residual interference and numerical instability (Marshoud et al., 2018).

In practice, VLC implementations of NOMA often adopt fixed or heuristic power allocation strategies. A common approach is weighted allocation proportional to the inverse of the user rank, where users are sorted by ascending channel gain. For example, assuming K users with ordered indices, weights $w_k = K - k + 1$ are normalized to yield transmit powers $p_k = w_k / \sum_{j=1}^{K} w_j \cdot P_t$, where P_t is the total LED power budget. This simple heuristic reflects the logic of allocating more power to more disadvantaged users without relying on full CSI accuracy.

Despite its conceptual simplicity, PD-NOMA faces key challenges in VLC environments. First, when user channels are too similar, common in uniform room lighting, SIC becomes unreliable and residual interference limits the rate of weaker users. Second, LED power constraints limit the feasible range of power allocations, especially under biasing and linearity restrictions. Third, SIC complexity scales linearly with the number of users, rendering full NOMA infeasible in dense deployments. Hybrid schemes combining Orthogonal Multiple Access (OMA) with NOMA have been proposed to mitigate this, but they introduce overhead in scheduling and grouping (S. Naser et al., 2020).

In summary, PD-NOMA offers improved spectral efficiency under favorable channel disparities and well-conditioned SIC chains, but is sensitive to geometric symmetry and LED hardware limitations. In contrast to spatial-domain schemes like SDMA, which rely on multiple transmit apertures and accurate CSIT, NOMA operates effectively even in overloaded regimes with

$K > N_t$, making it a compelling benchmark for RSMA-based designs explored in this thesis.

2.2.3 Rate-Splitting Multiple Access (RSMA)

RSMA unifies SDMA and NOMA within a single linear-precoding framework by allowing each user's message to be divided into a *common* part, decoded by all users, and a *private* part, decoded only by its intended receiver (Mao et al., 2018). The basic architecture of a two-user RSMA transmission model is illustrated in Figure 2.4.

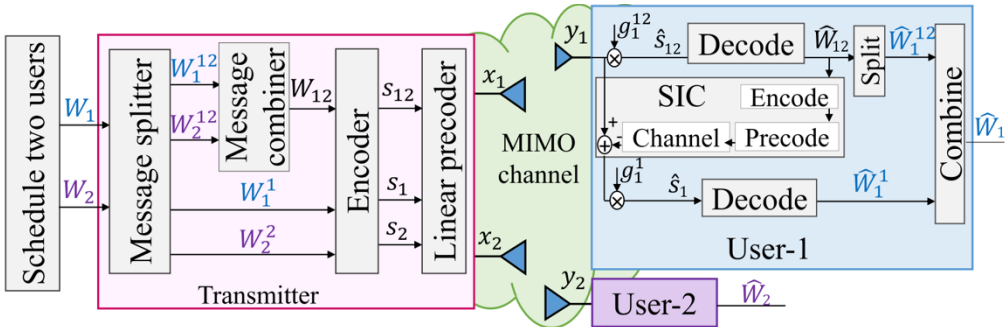

Figure 2.3: Two-user transmission model using RS (Mao et al., 2018).

The transmit signal in a K-user MU-MISO setting is therefore

$$\boldsymbol{x} = \boldsymbol{w}_c s_c + \sum_{k=1}^{K} \boldsymbol{w}_k \, s_k, \tag{2.2}$$

where s_c and s_k denote the common and kth private symbols, and $\boldsymbol{w}_c, \boldsymbol{w}_k \in \mathbb{R}^{N_t}$ are their precoders. Each PD first decodes the common stream while treating all private signals as noise, cancels it through a single SIC step, and finally decodes its own private stream. If $\boldsymbol{w}_c = 0$ the scheme collapses to SDMA; if the common stream carries the strong-channel user's data and private precoders are power-split in the usual NOMA order, RSMA behaves like PD – NOMA.

This hybrid interference-management philosophy offers two practical

benefits. First, robustness to imperfect CSIT: partial decoding of interference (via the common stream) mitigates the severe rate loss experienced by SDMA when spatial orthogonality is disturbed. Second, computational scalability; in 1-RSMA, only one SIC operation is needed, regardless of user count, which substantially lowers receiver complexity relative to full NOMA. These properties have made RSMA an appealing candidate for overloaded cellular deployments; the following section surveys how the concept has been translated to the unique optical-channel constraints of VLC.

2.2.4. RSMA for VLC: Literature Overview

RSMA has emerged as an effective multiple access technique for VLC systems, due to its capability to manage interference and improve spectral efficiency and fairness among users. In this literature survey, recent significant contributions on RSMA in VLC contexts are reviewed and critically analyzed.

Although this literature survey spans a broad spectrum of RSMA-based VLC research, the present thesis specifically focuses on 1-layer RSMA in single-cell indoor MISO VLC networks, with practical physical layer constraints. The wider context presented here situates this study within the evolving landscape of RSMA-VLC research, providing both motivation and justification for the design decisions and assumptions adopted in the subsequent chapters.

(Hu et al., 2023) provide a foundational review comparing RSMA, NOMA, and SDMA within multiple-input-multiple-output (MIMO) broadcast channels. While the application of RSMA to VLC remains in its early stages, the study explores its feasibility in Single Input Single Output VLC configurations. It questions whether RSMA can alleviate the complexity and SIC burden typically associated with NOMA. Although RSMA also relies on SIC, it offers a potentially more efficient alternative under certain conditions, inspired by the benefits observed in 1-layer RSMA for MISO scenarios.

Building upon the theoretical foundations of RSMA, (Ma et al., 2022) address two fundamental challenges in RSMA-aided VLC networks: the derivation of achievable rate bounds and the design of robust beamformers. The

study presents the first theoretical lower bound on achievable rates under practical VLC power constraints, including peak optical, average optical, and average electrical power limits. This bound is then utilized to guide the development of beamformer designs, which are shown through numerical evaluations to significantly outperform conventional approaches.

(Naser et al., 2020) offers a comprehensive overview of multiple access techniques in MIMO-VLC systems and introduces RSMA as a general framework encompassing both NOMA and SDMA. The paper presents preliminary results for a two-user MISO VLC scenario under per-LED power constraints, demonstrating RSMA's superiority in terms of weighted sum rate. Additionally, it outlines key technical challenges, such as non-linear distortion, security vulnerabilities, and ambient light interference, highlighting future research directions for practical RSMA deployment in VLC.

Expanding upon prior work, (S. A. Naser et al., 2021) investigates the application of RSMA in multi-cell MISO VLC systems under per-LED power constraints. After contextualizing RSMA as a superset of SDMA and NOMA in single-cell scenarios, the study proposes a coordinated beamforming (CB) design to enhance performance for cell-edge users. This work aims to improve indoor coverage and support user mobility in practical deployments.

In a recent study, (Liu et al., 2023) introduces a Genetic Algorithm (GA)-based approach to optimize the precoding matrix for RSMA in MU-MISO VLC systems. The paper also establishes essential SINR constraints for practical deployment. Simulation results show that RSMA achieves higher spectral efficiency than NOMA under specified conditions. Additionally, the study reveals that tighter SINR constraints reduce the weighted sum rate, underscoring the importance of maintaining feasible lower bounds for both common and private stream rates.

A comprehensive framework for integrating RSMA into multi-cell VLC systems is proposed in (S. Naser et al., 2022), with a particular focus on interference mitigation and complexity reduction. The study introduces a CB-based RSMA scheme for multi-cell MISO VLC networks to address inter-cell

interference, especially for cell-edge users. Simulation results demonstrate that RSMA outperforms CB-based SDMA in terms of robustness to imperfect CSI and system complexity. Although joint transmission yields the highest performance, the authors note its impracticality due to elevated communication overhead.

The trade-off between Energy Efficiency (EE) and Spectral Efficiency (SE) in RSMA-aided MISO VLC downlink systems is comprehensively analyzed in (Hu et al., 2024). The authors introduce Resource Efficiency as a flexible performance metric to balance EE and SE, formulating a maximization problem under Quality of Service (QoS) and LED operating constraints. The study further emphasizes that RSMA generalizes traditional access schemes, encapsulating NOMA and SDMA as boundary cases.

In (Rallis et al., 2023), an RSMA-inspired user cooperation strategy is introduced for hybrid VLC-RF networks, targeting coverage extension. The approach considers the use of users within the VLC cell as RF relays for those located outside its range. The study outlines how tuning the split between common and private message components allows for controlling system complexity and data throughput. RSMA is described as a framework that can generalize both NOMA and SDMA in RF and VLC contexts.

The work in (Xing et al., 2022) focuses on energy efficiency optimization in RSMA-based VLC systems, which has received less attention compared to spectral efficiency. The study emphasizes that RSMA's message-splitting structure introduces a power allocation trade-off between common and private streams, posing challenges for efficient resource optimization.

In (Girdher et al., 2024), the authors examine RSMA-based VLC networks incorporating Simultaneous Lightwave Information and Power Transfer (SLIPT) for IoT scenarios. They formulate a fairness-oriented optimization problem to maximize the minimum harvested energy across users, subject to DC bias and power constraints. Results indicate improved robustness and performance compared to NOMA and SDMA under various network load conditions.

(Guo et al., 2024) investigates resource allocation in multi-LED RSMA-based SLIPT VLC networks, aiming to enhance user fairness. By jointly optimizing the DC bias, precoding vectors, and common message rates, the authors seek to maximize the minimum rate (MMR) under constraints such as EH requirements and LED operation limits. Results suggest that RSMA improves both spectral and energy efficiency, though MMR performance declines with increasing user count and limited drive current.

(Nguyen et al., 2024) examines energy efficiency (EE) optimization in RSMA-based VLC systems transmitting confidential private messages. The study formulates an EE maximization problem that considers both the common rate and secrecy rate, addressing the design from a physical layer security perspective. Using the Dinkelbach algorithm and Convex-Concave Procedure, the analysis reveals that EE and common rate increase with channel similarity, whereas secrecy rate shows an inverse trend.

(Qiu et al., 2025) investigates RSMA-aided VLC networks under imperfect Channel State Information, focusing on two core challenges: establishing lower bounds on achievable rates and developing robust beamforming strategies. A theoretical lower bound for VLC channel capacity is derived, and a worst-case rate maximization approach is proposed using SDR, S-lemma, and CCP techniques. Simulation results show that the proposed scheme outperforms conventional SDMA and NOMA under practical CSI uncertainty, based on a 1-layer RSMA structure with SIC decoding.

(Maraqa et al., 2025) examines the integration of Reconfigurable Intelligent Surfaces (RIS) into VLC systems to improve physical layer security. The study formulates a joint optimization framework for access point power allocation, RIS association, and element orientation to maximize both the minimum secrecy rate and secrecy energy efficiency. A genetic algorithm is used to solve the resulting mixed-integer nonlinear problem. Results show that RSMA outperforms power-domain NOMA in terms of both spectral rate and spectral efficiency under diverse network conditions.

(Guo et al., 2025)investigates IRS-assisted MISO VLC networks

incorporating RSMA with a focus on physical layer security. The study formulates a Secrecy Energy Efficiency (SEE) maximization problem by jointly optimizing beamforming vectors, DC bias, common information rate, and IRS alignment. A deep reinforcement learning-based DS-PPO method is employed to address the non-convex problem. Results indicate that the integration of IRS and RSMA yields notable SEE gains compared to conventional schemes without IRS.

(Maraqa et al., 2024) proposes a novel indoor VLC system assisted by Optical Simultaneous Transmission and Reflection RIS to address LOS blockages and enable 360-degree coverage. The authors formulate a sum-rate maximization problem by jointly optimizing the refractive index and orientation angles of RIS elements, considering both RSMA and NOMA. Results show that the RSMA-based system consistently outperforms its NOMA counterpart in terms of sum rate and energy efficiency. This work constitutes the first technical evaluation of OSTAR-RIS under the RSMA framework.

(Salam et al., 2025) investigates Optical IRS-assisted Underwater Wireless Optical Communication (UWOC) systems, with a focus on scenarios lacking direct LOS paths. The study examines the application of RSMA in UWOC under turbulence-induced fading and pointing errors. Reported findings suggest that RSMA offers improved resilience to such impairments, contributing to higher system capacity and lower outage probability. The work situates RSMA among several multiple access techniques under consideration for next-generation UWOC systems.

(Prabhakar et al., 2024) presents a comparative analysis of Terahertz and Visible Light Communication (VLC) systems under the influence of weather conditions and static human blockages. The study evaluates multiple access techniques, including RSMA, by deriving expressions for the Signal-to-Interference-plus-Noise Ratio (SINR) and achievable rates of both common and private streams. Emphasis is placed on modeling the blockage environment and assessing the effects of environmental impairments on system performance across different access schemes.

(Kowshik et al., 2024) proposes a twin-tiered deep learning architecture named ViRSMALNet, tailored for multi-user MIMO RSMA-based VLC systems. The architecture utilizes two parallel Long Short-Term Memory (LSTM) neural networks to jointly decode common and private streams, eliminating the need for SIC. Simulation results show that ViRSMALNet surpasses traditional LS and MMSE detectors and performs comparably to optimal maximum likelihood detection in terms of symbol error rate. Additionally, the study analyzes how system and network parameters such as the number of LEDs, photodetectors, and neural hyperparameters influence performance. This constitutes the first implementation of an LSTM-based RSMA receiver in the VLC domain.

A comparative summary of the key RSMA–VLC studies discussed above, including their network configurations, modeled imperfections, and optimization goals, is presented in Table 2.1.

2.3 IDENTIFIED RESEARCH GAPS

Despite the breadth of studies surveyed above and summarized in Table 2.1, four open issues remain unaddressed in current RSMA–VLC research and motivate the technical directions taken in this thesis.

First, the majority of RSMA–VLC works adopt simplified optical hardware assumptions that neglect the nonlinear relationship between LED drive current and light intensity, or decouple illumination constraints from transmission power limits. Without a unified and physically valid model, it becomes difficult to assess whether theoretical SE gains are realizable in practice. In response, this thesis, formulates an end-to-end system model that simultaneously enforces LED current linearity, illuminance requirements, and transmit-power constraints under a Lambertian propagation model.

Second, comparative evaluations of RSMA often omit realistic baselines. While RSMA is frequently contrasted with theoretical SDMA or ideal OMA schemes, practical implementations of power-domain NOMA remain underexplored,

Table 2.1: Representative RSMA–VLC studies and their key characteristics.

Reference	Scenario	Constraints	Optimization / Metric
S. Naser et al. (2020)	2-User Single-Cell MISO	Per-LED optical-power limits	Weighted sum rate
Ma et al. (2022)	Single-cell MISO	Peak / avg. optical & electrical power	Robust SE (closed-form bound)
S. A. Naser et al. (2021)	Multi-cell MISO	Inter-cell interference; per-LED power	Cell-edge SE
Liu et al. (2023)	Single-cell MISO	Target SINR per user	Spectral efficiency
S. Naser et al. (2022)	Multi-cell MISO	Imperfect CSIT	Robust SE
Xing et al. (2022)	Single-cell MISO	Common/private power-split trade-off	Energy efficiency
Hu et al. (2024)	Multi-cell MISO	QoS; LED drive limits	Resource Efficiency (EE–SE)
Rallis et al. (2023)	Hybrid VLC–RF	Coverage holes outside VLC cell	Complexity vs. throughput
Girdher et al. (2024)	SLIPT MISO	DC bias; EH demand	Max–min harvested energy
Guo et al. (2024)	Multi-LED SLIPT	EH targets; LED limits	Max–min rate fairness
Nguyen et al. (2024)	Single-cell MISO	Secrecy constraints	EE with secrecy
Prabhakar et al. (2024)	THz vs. VLC	Weather / blockage models	SINR & achievable rate
Kowshik et al. (2024)	Multi-user MIMO	SIC complexity	Symbol error rate
Maraqa et al. (2024)	OSTAR-RIS indoor VLC	LoS blockage; 360° coverage	Sum rate
Maraqa et al. (2025)	RIS-assisted MISO	RIS orientation + power split	Min. secrecy rate & SEE
Guo et al. (2025)	IRS-assisted MISO	SEE target	Secrecy energy efficiency
Qiu et al. (2025)	Single-cell MISO	Imperfect CSIT	Worst-case rate
Salam et al. (2025)	Optical IRS-UWOC	Turbulence; pointing error	Capacity & outage
This thesis (2025)	Multi-cell MU-MISO	Full hardware & illumination constraints, spatial randomness	Comprehensive SE benchmarking, spatial analysis

particularly under VLC-specific constraints such as SIC stability and LED saturation. This thesis, therefore implements an optimized PD-NOMA baseline using channel-aware MRT precoding and inverse-rank power allocation, enabling direct benchmarking of RSMA against NOMA across various power levels and user counts.

Third, prior RSMA–VLC studies predominantly assume that all users are positioned within overlapping LED footprints, where the received optical power is balanced across multiple transmitters, or assume only some fixed user positioning. This assumptions, while analytically convenient, does not reflect

realistic deployments in which users may be arbitrarily placed across the room, potentially outside LED overlap regions. This thesis, removes this restriction by distributing users randomly over the entire floor area, allowing the emergence of single-LED dominant channels. This broader configuration captures more realistic user geometries and reveals how RSMA adapts its rate structure, often favoring the common stream, under increasing transmit power levels.

Fourth, performance evaluation in VLC is typically limited to Monte Carlo analysis over randomized user positions. While statistically valid, this approach obscures spatial patterns and fails to reveal performance sensitivity to user placement. This thesis, complements conventional MC evaluation with a structured spatial sweep, where one user is fixed and the second is systematically moved across the room. The resulting heat-maps provide visual insight into how SE varies with geometry, enabling practical cell-design recommendations based on RSMA's robustness to spatial asymmetries.

These gaps collectively delineate the research agenda pursued in this thesis and justify the methodological choices presented in Chapters 3–5.

CHAPTER 3

3. SYSTEM MODEL

This chapter defines the system model and physical-layer assumptions used throughout the thesis. To support different evaluation objectives, two complementary simulation configurations are considered. The first configuration aims to assess average system performance across a range of power budgets and user densities; in this case, multiple users are placed randomly throughout the entire room area in each Monte Carlo trial, enabling statistical comparisons between RSMA and NOMA under realistic spatial variability. The second configuration, by contrast, focuses on spatial sensitivity: one user is fixed at a representative location while a second user is swept across a dense spatial grid to generate heatmaps of spectral efficiency. These two configurations share a common transmission and optimization framework, but differ in how user locations are instantiated and interpreted. The sections that follow detail the unified signal model, optical channel, and transmission constraints employed in both configurations.

3.1 PHYSICAL ENVIRONMENT

This thesis considers a downlink indoor VLC system consisting of multiple ceiling-mounted LEDs serving multiple user terminals equipped with single PDs. The communication takes place in a typical rectangular room with a fixed height, where the LED arrays are placed symmetrically on the ceiling and users are randomly distributed within the illuminated area. This setup is illustrated in Figure 3.1, showing the room geometry, LED positions, and user plane configuration. The complete list of system-level parameters used in the simulations is provided in Chapter 4.

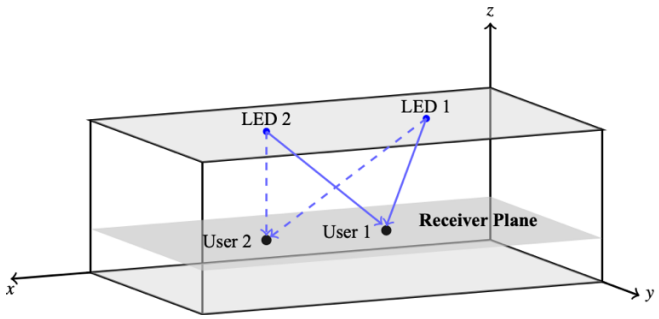

Figure 3.1: Multi User MISO Indoor VLC System Model.

The system adopts a MU-MISO configuration, where the central transmitter, composed of N_t LEDs, simultaneously transmits independent data streams to K users through IM/DD. Each user is equipped with a single PD, forming the MISO channel structure required for spatial multiplexing and interference management.

All users are assumed to lie on a fixed horizontal plane (e.g., tabletop level), and their positions remain constant during each simulation instance. Over multiple iterations, user locations are updated according to the simulation configuration, either via random sampling (Monte Carlo) or systematic spatial sweeping. A direct LOS path is assumed between each LED and user, while reflections and diffuse propagation are neglected, consistent with the LOS-dominated nature of indoor VLC channels.

To ensure practical feasibility, LED operation is constrained within its linear region, with the average optical power and peak current constrained by hardware specifications. User locations and channel gains vary across multiple Monte Carlo realizations, enabling performance evaluation under a wide range of spatial configurations.

In this setup, RSMA is applied at the transmitter to manage inter-user interference and enhance spectral efficiency. The transmitted signals are precoded based on the estimated CSI and delivered through the LED array. At the receiver side, PDs perform direct detection to recover the transmitted signals, followed by a decoding process that separates the common and private stream components as specified by the RSMA protocol.

3.2 LAMBERTIAN LOS CHANNEL MODEL

In this study, only direct LOS components are considered for optical wireless channel modeling. Due to the highly directional and quasi-static nature of indoor VLC propagation, diffuse and non-LOS components are neglected. Each LED is modeled as a Lambertian source of order m, where m is related to the semi-angle at half power $\Phi_{1/2}$ as:

$$m = \frac{-\ln(2)}{\ln\left(\cos\left(\Phi_{1/2}\right)\right)} \tag{3.1}$$

The geometric configuration of a typical Lambertian VLC link, including the relevant angular and distance parameters, is illustrated in Figure 3.2. The irradiance angle $\phi_{k,j}$ and incidence angle $\psi_{k,j}$ characterize the orientation between the LED and the PD, while $d_{k,j}$ denotes the Euclidean distance between them.

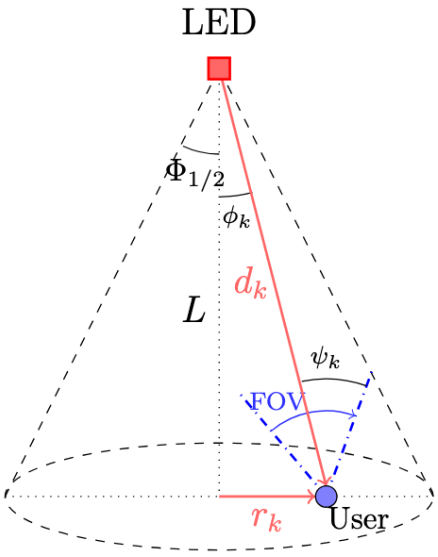

Figure 3.2: Lambertian radiation model with LOS.

The channel gain between LED j and user k is defined as:

$$h_{k,j} = \begin{cases} \frac{(m+1)A_{\text{PD}}}{2\pi d_{k,j}^2} \cos^m(\phi_{k,j}) T_f r_{oe} g(\psi_{k,j}) \cos(\psi_{k,j}), & \psi_{k,j} \le \Psi_c \\ 0, & \text{otherwise} \end{cases} \quad (3.2)$$

where,

- A_{PD}: physical area of the PD,
- $d_{k,j}$: Euclidean distance between LED j and user k,
- $\phi_{k,j}$: irradiance angle (LED to PD),
- $\psi_{k,j}$: incidence angle (PD to LED),
- Ψ_c: PD FOV,
- T_f: optical filter gain,
- $g(\psi)$: concentrator gain.
- r_{oe}: optical-electrical conversion efficiency constant

Moreover, the concentrator gain is defined as:

$$g(\psi) = \begin{cases} \frac{n^2}{\sin^2(\Psi_c)}, & 0 \le \psi \le \Psi_c \\ 0, & \text{otherwise} \end{cases} \quad (3.3)$$

Where n is the refractive index of the concentrator.

For each user–LED pair, the DC gain $h_{k,j}$ is computed using Equation 3.2. The resulting channel matrix is constructed as:

$$\mathbf{H} \in \mathbb{R}^{N_r \times N_t}, \quad \mathbf{H} = \begin{bmatrix} h_{1,1} & h_{1,2} \\ \vdots & \vdots \\ h_{N_r,1} & h_{N_r,2} \end{bmatrix} \quad (3.4)$$

This channel matrix is used directly in RSMA signal modeling and optimization. While $\mathbf{H}$ captures only the physical user–LED paths and thus has N_r rows, the total number of transmitted streams in the RSMA system is $N_r + 1$, including one common stream and N_r private streams. This distinction is reflected in the dimension of the precoding matrix $\mathbf{W} \in \mathbb{R}^{N_t \times (N_r+1)}$, which operates on the augmented signal vector $\boldsymbol{s} \in \mathbb{R}^{N_r+1}$.

3.3 DEVICE & ILLUMINATION CONSTRAINTS

Due to physical limitations of the LED drivers, the instantaneous electrical current applied to each LED must remain within its linear operating range. This constraint is enforced by bounding the ℓ_1-norm of each row of the precoding matrix:

$$\|\omega_i\|_1 \leq I_{lim}, \quad \forall i \in \{1, \dots, N_t\} \tag{3.5}$$

where ω_i denotes the i-th row of the precoding matrix $\mathbf{W}$, and I_{lim} represents the maximum allowable AC signal amplitude imposed on each LED. This condition ensures that the superposition of all stream components entering an LED does not exceed the safe dynamic range of the driver circuitry.

In VLC systems based on IM/DD, the optical transmit signal must remain non-negative. This is handled by introducing a DC-bias vector $\mathbf{d}$ and constraining the precoded signal accordingly:

$$\mathbf{x} = \mathbf{W}\mathbf{s} + \mathbf{d} \geq 0 \tag{3.6}$$

While the non-negativity is not explicitly enforced as an optimization constraint in our formulation, the precoding matrix $\mathbf{W}$ is initialized and scaled to ensure that this condition is satisfied throughout all simulation runs.

3.4 RSMA SIGNAL MODEL

In the considered RSMA-VLC system, the transmitter simultaneously serves N_r users using N_t LEDs. A total of $N_r + 1$ information-bearing streams are transmitted: one common stream s_0 intended to be decoded by all users, and N_r private streams $\{s_k\}_{k=1}^{N_r}$, each targeted to a specific user.

Let $s \in \mathbb{R}^{N_r+1}$ denote the vector of real-valued, zero-mean information symbols:

$$\mathbf{s} = \left[\mathrm{s}_0, \mathrm{s}_1, \ldots, \mathrm{s}_{N_r}\right]^{\mathrm{T}}$$

Each stream s_k is linearly precoded by a beamforming vector $w_k \in \mathbb{R}^{N_t}$, and the overall precoding matrix is defined as:

$$\mathbf{W} = \left[\mathbf{w}_0 \mid \mathbf{w}_1 \mid \ldots \mid \mathbf{w}_{N_r}\right] \in \mathbb{R}^{\mathrm{N_t} \times (\mathrm{N_r}+1)}$$

The optical transmit signal, which must satisfy the real-valued and non-negative constraints of intensity modulation, is defined as:

$$\mathbf{x} = \mathbf{W}\mathbf{s} + \mathbf{d} \tag{3.7}$$

where $d \in \mathbb{R}^{N_t}$ is a fixed DC-bias vector added to ensure non-negativity:

$$\mathbf{x} \geq 0$$

The received signal at user k is given by:

$$\mathrm{y_k} = \mathbf{h}_k^T \mathbf{x} + \boldsymbol{n}_k \tag{3.8}$$

where,

- $\mathbf{h}_k^T \in \mathbb{R}^{1 \times N_t}$ is the k-th row of the channel matrix $\mathbf{H}$,
- $n_k \sim \mathcal{N}(0, \sigma^2)$ denotes AWGN noise.

The signal component $\mathbf{h}_k^T\mathbf{W}\mathbf{s}$ contains both common and private streams. SIC is employed at each user to decode the common stream first, followed by its own private stream, treating all others as interference. The SINR and rate expressions are detailed in Section 4.1.1.

3.5 BASELINE PD-NOMA SCHEME

To provide a meaningful benchmark for the proposed RSMA system, a PD-NOMA architecture is implemented under the same physical and optical constraints. For each channel realization, users are first sorted in ascending order of channel strength, measured by the ℓ_1-norm of their channel gain vectors. The weakest user is assigned the largest power portion and decoded first, ensuring proper SIC at the receivers.

The total optical power P_t is partitioned using a fixed weighting strategy: the user ranked i in the sorted order receives power proportionally to $N_r + 1 - i$. This allocation favors weaker users to improve their SINR and supports successful SIC decoding. Precoding vectors are designed using MRT, where the beam for user k is aligned with its channel direction as $\mathbf{w}_k = \mathbf{h}_k \,/\, \|\mathbf{h}_k\|_2$. The full precoder matrix $\mathbf{W}$ is then scaled uniformly to satisfy the per-LED current constraint.

Once the MRT precoders and power levels are assigned, each user performs SIC by decoding signals of users with lower indices and subtracting them. The SINR of user k_i in position \$i\$ of the decoding order is given by:

$$\gamma_{k_i} = \frac{|\mathbf{h}_{k_i}^\top \mathbf{w}_{k_i}|^2 p_{k_i}}{\sigma^2 + \sum_{j=i+1}^{N_r} |\mathbf{h}_{k_i}^\top \mathbf{w}_{k_j}|^2 p_{k_j}} \tag{3.9}$$

where $p_{k_i}$is the allocated power for user k_i. The spectral efficiency of each user is computed as $R_{k_i} = \log_2(1 + \gamma_{k_i})$, and the total system spectral efficiency is obtained by summing over all users. This implementation aligns with the principles in (Marshoud et al., 2018).

CHAPTER 4

4. OPTIMIZATION & SIMULATION METHODS

4.1 RSMA OPTIMIZATION FRAMEWORK

Although the exact channel capacity of the IM/DD-based optical communication system is still an open problem without a closed-form solution, prior works have proposed theoretical bounds under certain input signal assumptions (Jiang et al., 2018). When the visible-light signal input distribution is modeled using truncated Gaussian or discretely spaced uniform distributions, several studies have demonstrated achievable rate bounds associated with constant factors, such as $\frac{e}{2\pi}$, $\frac{1}{2\pi e}$, and $\frac{2}{\pi e}$, under varying SNR or SINR constraints (Chaaban et al., 2016; Lapidoth et al., 2009; Shen et al., 2016, 2017; Zhou & Zhang, 2019). These constants arise from different assumptions and analytical approximations and serve as scaling factors in practical capacity formulations.

It is important to note that these constants do not influence the subsequent optimization process conducted in this study. Instead, our numerical framework operates on the structural consistency of achievable rate expressions, which preserve the foundational form of the classical Shannon capacity, adapted to the characteristics of VLC channels.

4.1.1 SINR and Rate Expressions

Based on the 1-RSMA signal model described in Section 3.4, the achievable rates are derived using the signal-to-interference-plus-noise ratios (SINRs) corresponding to the decoding of the common and private streams.

Each user first decodes the common stream s_0 by treating all private streams as interference. The SINR for decoding s_0 at user k is given by:

$$\gamma_{c,k} = \frac{|\mathbf{h}_k^T \mathbf{w}_0|^2 p_0}{\sum_{j=1}^{N_r} |\mathbf{h}_k^T \mathbf{w}_j|^2 p_j + \sigma^2} \tag{4.1}$$

The corresponding achievable common rate is:

$$R_{c,k} = \log_2(1 + \gamma_{c,k}) \tag{4.2}$$

To guarantee successful decoding at all receivers, the effective common rate is constrained by the worst-case user:

$$R_c = \min_{k \in \{1,\ldots,N_r\}} R_{c,k} \tag{4.3}$$

After removing s_0 via SIC, each user decodes its own private stream s_k while treating all remaining private streams as noise. The SINR for user k's private stream is:

$$\gamma_{p,k} = \frac{|\mathbf{h}_k^T \mathbf{w}_k|^2 p_k}{\sum_{j=1, j\neq k}^{N_r} |\mathbf{h}_k^T \mathbf{w}_j|^2 p_j + \sigma^2} \tag{4.4}$$

and the corresponding private rate is:

$$R_{p,k} = \log_2(1 + \gamma_{p,k}) \tag{4.5}$$

The total system sum-rate, which serves as the performance metric to be maximized, is expressed as:

$$R_{\text{tot}} = R_c + \sum_{k=1}^{N_r} R_{p,k} \tag{4.6}$$

4.1.2 Optimization Constraints

In addition to the hardware and illumination-related limitations introduced in Section 3.3 namely the LED forward-current bounds and the signal non-negativity constraint, several additional constraints arise in the context of rate

optimization. These include a total optical power budget, minimum power allocation per stream, and structural properties of the RSMA precoding architecture. Together, these form a constraint set that reflects both the physical feasibility of VLC hardware and the mathematical conditions necessary for a well-posed, stable optimization process.

These constraints are collectively incorporated into the joint precoder–power allocation problem and are enforced numerically during the solution process via MATLAB's interior-point algorithm.

The value of I_{lim} in Equation 3.5 determined by the linear region of the LED, which is bounded below and above by the minimum and maximum current levels, denoted by I_L and I_U, respectively. The system operates around a fixed DC bias current I_{DC}, and thus the allowable swing for the modulated signal is calculated as:

$$I_{\text{lim}} = \min(I_{\text{DC}} - I_L,\ I_U - I_{\text{DC}}) \tag{4.7}$$

This definition guarantees that the modulated signal remains within the linear dynamic region of the LED regardless of the bias point, avoiding signal distortion or clipping. Here, I_{DC} is typically chosen to lie at the midpoint of $[I_L,\ I_U]$ to maximize the usable range symmetrically.

The total optical power transmitted across all streams must not exceed the system's power budget. This is modeled by a quadratic constraint on the stream amplitudes:

$$\sum_{k=0}^{N_r} p_k^2 \leq P_t \tag{4.8}$$

where p_k denotes the amplitude scaling factor for stream k. This constraint reflects both illumination requirements and hardware safety limits in high-power VLC transmitters.

To avoid degenerate solutions in which certain streams are assigned negligible power, a minimum power threshold is imposed:

$$p_k^2 \geq p_{min} P_t, \quad \forall k \in 1, \ldots, N_r \tag{4.9}$$

This constraint ensures that each private stream maintains a baseline energy level proportional to the total transmit power P_t, thereby preserving sufficient optical intensity for reliable detection. Notably, no such lower bound is enforced on the common stream, allowing the optimizer to flexibly reduce its power when advantageous.

4.1.3 Objective Function

The goal of the optimization is to maximize the total spectral efficiency of the VLC-RSMA system while satisfying all hardware and physical constraints introduced above. The total rate is defined as:

$$R_{\text{tot}} = R_c + \sum_{k=1}^{N_r} R_{p,k} \tag{4.10}$$

where R_c is the minimum decodable common rate across all users, and $R_{p,k}$ denotes the private rate for user k.

Due to the coupled SINR expressions and nonlinear constraint set, the optimization problem is non-convex. It is solved numerically using MATLAB's `fmincon` solver with the interior-point algorithm, which supports nonlinear objectives and inequality constraints.

The optimization jointly determines the precoding matrix $W \in \mathbb{R}^{N_t \times (N_r+1)}$ and the power allocation vector $p \in \mathbb{R}^{N_r+1}$. Since `fmincon` minimizes a scalar objective, the original maximization is reformulated as:

$$\min_{W,p} -R_{\text{tot}} \tag{4.11}$$

4.1.4 Final Problem Statement

The complete joint precoding and power allocation problem is summarized below. The objective is to maximize the total achievable rate R_{tot} under all system and hardware constraints:

$$\max_{\mathbf{W},\mathbf{p}} R_c + \sum_{k=1}^{N_r} R_{p,k} \tag{4.12a}$$

$$\text{s.t. } \|\omega_i\|_1 \leq I_{\text{lim}} \tag{4.12b}$$

$$\sum_{k=0}^{N_r} p_k^2 \leq P_t \tag{4.12c}$$

$$p_k^2 \geq p_{\min} P_t \tag{4.12d}$$

$$\mathbf{x} = \mathbf{W}\mathbf{s} + \mathbf{d} \geq 0 \tag{4.12e}$$

$$\mathbf{h} \propto (3.2) \tag{4.12f}$$

This non-convex optimization problem is solved numerically using a constrained nonlinear solver, as described in the previous section.

4.2 INITIALIZATION STRATEGY

Before optimization begins, a feasible starting point for the precoder matrix $\mathbf{W}$ and power vector $\mathbf{p}$ must be specified. In this work, we adopt a randomized yet constraint-aware initialization strategy to support robust convergence under interior-point methods.

Each row of the precoding matrix $W \in \mathbb{R}^{N_t \times (N_r+1)}$is initialized with independent Gaussian entries and then normalized such that the ℓ_1-norm of each row equals half the maximum allowable per-LED current:

$$\left\| \mathbf{w}_i^{(0)} \right\|_1 = 0.5 \times I_{lim}, \quad \forall \mathrm{i} \in \{1, \ldots, \mathrm{N_t}\}. \tag{4.13}$$

This normalization ensures that all rows start well within the feasible region, providing sufficient margin from constraint boundaries while avoiding zero-valued or highly symmetric starting points that may hinder optimization.

The initial power allocation vector $p \in \mathbb{R}^{N_r+1}$ is set uniformly across the common and private streams:

$$p_k^{(0)} = \frac{P_t}{N_r + 1}, \quad \forall k \tag{4.14}$$

This satisfies the total transmit power constraint exactly and keeps each power coefficient well above the minimum threshold required by the system.

Together, this initialization ensures that both feasibility and symmetry-breaking are enforced from the outset, enabling stable convergence of the interior-point solver used by `fmincon`.

4.3 SIMULATION SETUP

This section outlines the simulation configurations used to evaluate the proposed RSMA framework under various user geometries and system parameters. In all cases, the optimization routine is solved using MATLAB's `fmincon` with interior-point method, initialized as described in Section 4.2. System parameters remain fixed throughout and are listed in Table 4.1.

To evaluate the performance of the proposed RSMA-based VLC system, two complementary simulation configurations are designed.

- **Configuration 1 – Random-Placement Benchmark:** This setup assesses average SE across varying transmit power levels and user counts. For each configuration, 1000 Monte Carlo iterations are performed, where user positions are randomly sampled over the entire floor area (see: Figure 4.1). RSMA optimization is executed for each iteration, and results are averaged. A PD-NOMA baseline is also simulated under the same user positions for direct benchmarking. The procedure is summarized in Algorithm 1.

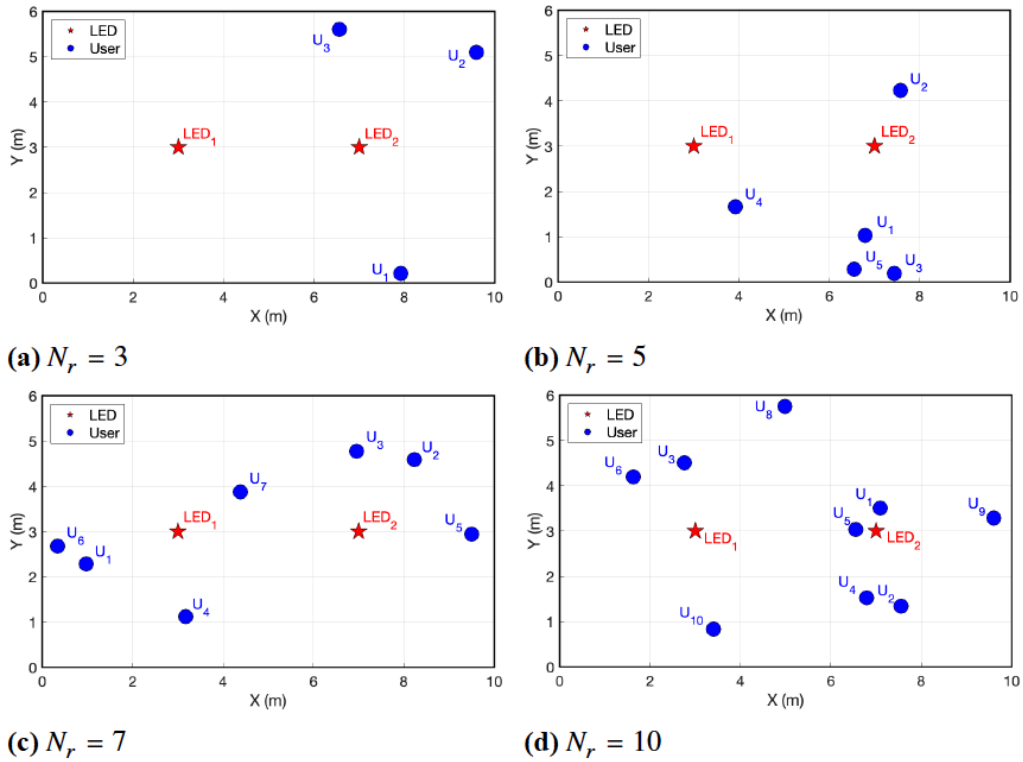

Figure 4.1: Representative user layouts for Configuration 1.

- **Configuration 2 – Spatial Sensitivity Analysis:** To investigate the spatial behavior of RSMA, a second user is swept across a dense grid while the first user remains fixed (Figure 4.2). This configuration is repeated for three representative fixed-user placements:

  Scenario i: The fixed user is near the room edge.
  Scenario ii: The fixed user is directly below the first LED.
  Scenario iii: The fixed user is centered between the two LEDs.

  At each grid point, optimization is repeated with 10 Monte-Carlo runs to average out channel variations. The resulting spectral-efficiency maps reveal how geometry influences RSMA behavior. The procedure is summarized in Algorithm 2.

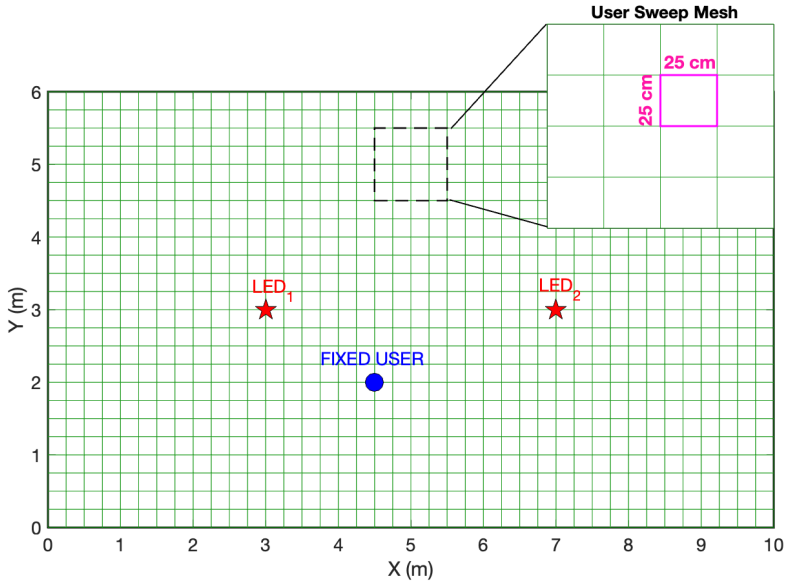

Figure 4.2: Sweep mesh used in *Scenario iii* of Configuration 2.

Table 4.1: Simulation Parameters for the Indoor VLC-RSMA System

Parameter	**Symbol**	**Value**
Photodiode area	A_{PD}	$10^{-4}\,\text{m}^2$
Semi-angle at half power	$\Phi_{1/2}$	60°
Field of view	Ψ_{FOV}	80°
Refractive index	n	1.5
Optical filter gain	T_s	1
Optical-to-electrical conversion	r_{oe}	0.53 A/W
Min/Max/Avg LED current	I_L, I_U, I_{DC}	0.2 A, 1.0 A, 0.6 A
Number of LEDs	N_t	2
Number of users	N_r	2 ~ 7
Room dimensions	–	$10 \times 6 \times 3.5\,\text{m}^3$
LED positions	–	$(3, 3, 3.5)$ and $(7, 3, 3.5)$
Receiver plane height	z	1.0 m
PSD of noise	N_0	$10^{-21}\,\text{A}^2/Hz$
Noise variance	σ^2	2×10^{-14}
Channel bandwidth	B	20 MHz
Transmit power	P_t	varies (e.g., 35 dBm $\approx$ 3.16 W)
Mininum required power	p_{min}	0.1

Algorithm 1: Monte-Carlo Simulation Framework for Configuration 1

Input: System parameters, user counts N_r, transmit-powers P_t, Monte–Carlo trials M

Output: Monte-Carlo averages $\overline{\mathrm{SE}}_{\mathrm{RSMA}}$, $\overline{R}_c$, $\overline{\mathbf{R}}_p$, and $\overline{\mathrm{SE}}_{\mathrm{NOMA}}$

for $i = 1$ **to** I **do**
  $N_r \leftarrow N_r^i$
  for $j = 1$ **to** J **do**
    $P_t \leftarrow P_t^j$;
    Initialize accumulators $\Sigma_{SE_{RSMA}}, \Sigma_{R_c}, \Sigma_{\mathbf{R}_p}, \Sigma_{SE_{NOMA}} \leftarrow 0$
    for $m = 1$ **to** M **do**
      1) User placement: draw $\mathbf{u}_k \sim \mathcal{U}([0, L_x]\times[0, L_y])$, $z_k = 1$ m
      2) Channel: build LOS matrix $\mathbf{H} \in \mathbb{R}^{N_t \times N_r}$ via (3.2)
      3) RSMA optimization:
        Initialization: choose feasible $\mathbf{W}^{(0)}$, $\mathbf{p}^{(0)}$ via (4.13-4.14)
        Solve Problem (4.12) using interior-point solver
        Obtain R_c, R_p, $\mathrm{SE}_{\mathrm{RSMA}}$
        4) NOMA baseline: evaluate PD-NOMA sum-SE via successive SIC (see Section 3.5)
        5) Accumulate: $\Sigma_{SE_{\mathrm{RSMA}}} += \mathrm{SE}_{\mathrm{RSMA}}$,
        $\Sigma_{R_c} += R_c$,
        $\Sigma_{R_p} += R_p$,
        $\Sigma_{SE_{\mathrm{NOMA}}} += \mathrm{SE}_{\mathrm{NOMA}}$
    6) Average over trials: $\overline{\mathrm{SE}}_{\mathrm{RSMA}}(i,j) = \Sigma_{SE_{\mathrm{RSMA}}}/M$,
    $\overline{R_c}(i,j) = \Sigma_{R_c}/M$,
    $\overline{R}_p(i,j) = \Sigma_{R_p}/M$,
    $\overline{\mathrm{SE}}_{\mathrm{NOMA}}(i,j) = \Sigma_{SE_{\mathrm{NOMA}}}/M$

return all averaged performance metrics

Algorithm 2: Monte-Carlo Simulation Framework for Configuration 2

Input: System parameters, fixed user location $\mathbf{u}^{\text{fix}}$, transmit power P_t, rectangular grid $\mathcal{G} = \{(x_g, y_g)\}$, Monte-Carlo trials M.

Output: Spatial RSMA sum-rate map $\text{SE}_{\text{avg}}(x_g, y_g)$.

Initialize matrix SE_{avg} with zeros, sized as $\mathcal{G}$

foreach $(x_g, y_g) \in \mathcal{G}$ **do**

  Initialize accumulator $\Sigma_{\text{SE}} \leftarrow 0$

  for $m = 1$ **to** M **do**

    1) User set: $\mathbf{U} = \{\mathbf{u}^{\text{fix}}, \sim \mathcal{U}([x_g, y_g]), z_k = 1\}$

    2) Channel: compute LOS matrix $\mathbf{H} \in \mathbb{R}^{2\times 2}$ via (3.2)

    3) RSMA optimization: Same with Algorithm 1

    4) Accumulate: $\Sigma_{\text{SE}} += \text{SE}_m$

  5) Monte-Carlo average: $\text{SE}_{\text{avg}}(x_g, y_g) = \Sigma_{\text{SE}}/M$

return SE_{avg}

CHAPTER 5

5. RESULTS & DISCUSSION

This chapter presents the numerical results obtained from the two simulation configurations outlined in Chapter 4 and interprets their implications for downlink VLC system design. Configuration 1 quantifies average SE across a range of transmit–power levels and user densities and benchmarks RSMA against PD-NOMA. Configuration 2 maps the spatial sensitivity of RSMA by sweeping a second user across the room for three representative fixed-user locations. Unless stated otherwise, all results adopt the system parameters in Table 4.1.

5.1 RESULTS FROM CONFIGURATION 1

The impact of the optical transmit power on the system throughput is first examined. Figure 5.1 compares the sum SE achieved by one–layer RSMA (1-RSMA) and PD-NOMA as P_t increases from 35 dBm to 65 dBm for four representative user loads ($N_r \in \{2, 3, 5, 7\}$). Across the lower–to–mid power range both schemes display an almost linear SE growth, consistent with operation in the high-SINR, interference-dominated regime of visible-light channels. Beyond approximately 60 dBm, however, the 1-RSMA curve begins to flatten and forms a shallow dome. This behavior is caused by the per-LED current ceiling I_{lim}; once any LED hits that limit, so the marginal SINR, and hence the SE, no longer scales linearly with P_t.

1-RSMA nonetheless outperforms PD-NOMA for every N_r; the absolute gain broadens with P_t, and reaches approximately 16.5 bps/Hz ($\approx 80\ \%$) at $P_t = 65$ dBm for the seven-user case. The slope of each curve rises with the number of users, indicating that multi-user diversity is effectively exploited in both schemes, yet the RS method leverages this diversity more efficiently,

particularly at intermediate loads ($N_r = 3 - 5$) where inter-user interference is strongest.

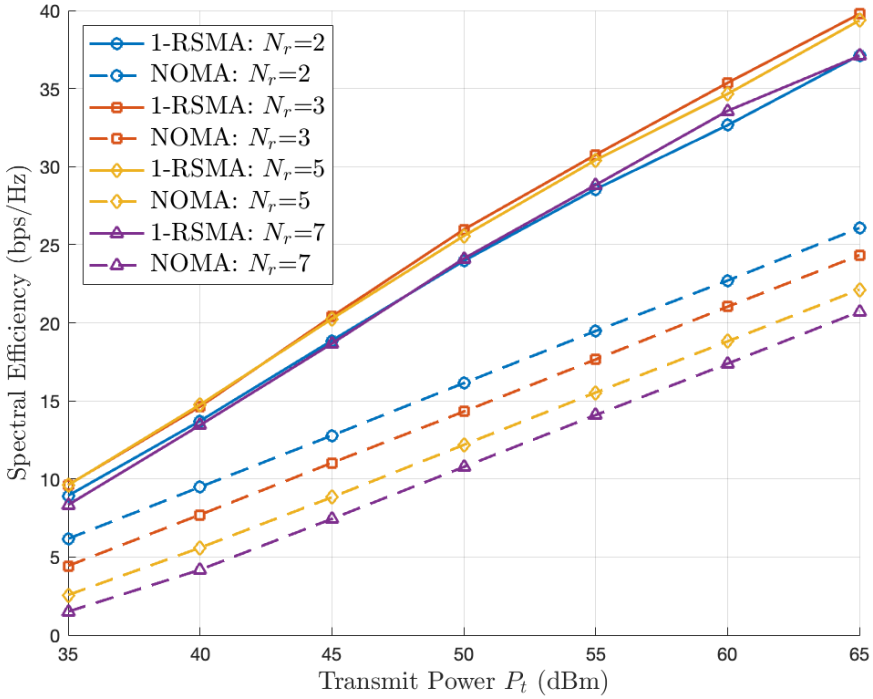

Figure 5.1: Sum spectral efficiency of one-layer RSMA and PD-NOMA versus transmit power $\boldsymbol{P_t}$ for $\boldsymbol{N_r} \in \{\mathbf{2}, \mathbf{3}, \mathbf{5}, \mathbf{7}\}$ users.

Figure 5.2 illustrates how the sum SE delivered by 1-RSMA evolves with the number of active users, $N_r = 2 - 8$, under four optical power budgets ($P_t \in \{0.5, 1.0, 1.5, 2.0\}$ W).

For every power level the SE first rises as additional users introduce MU diversity; the peak occurs at $N_r \approx 3 - 4$ where 1-RSMA can still balance common and private streams without severe power dilution. Beyond that point, the curves bend downward, reflecting two compounding factors (i) the available transmit power must be spread across a larger set of private streams, lowering the per-stream SINR, and (ii) the per-LED current ceiling I_{lim} caps the admissible modulation amplitude, so further increases in P_t cannot translate into proportional SINR gains. At the highest budget ($P_t = 2.0$) W, the maximum throughput 8.1 bps/Hz is observed at $N_r = 3$; by contrast, operating at ($N_r = 8$

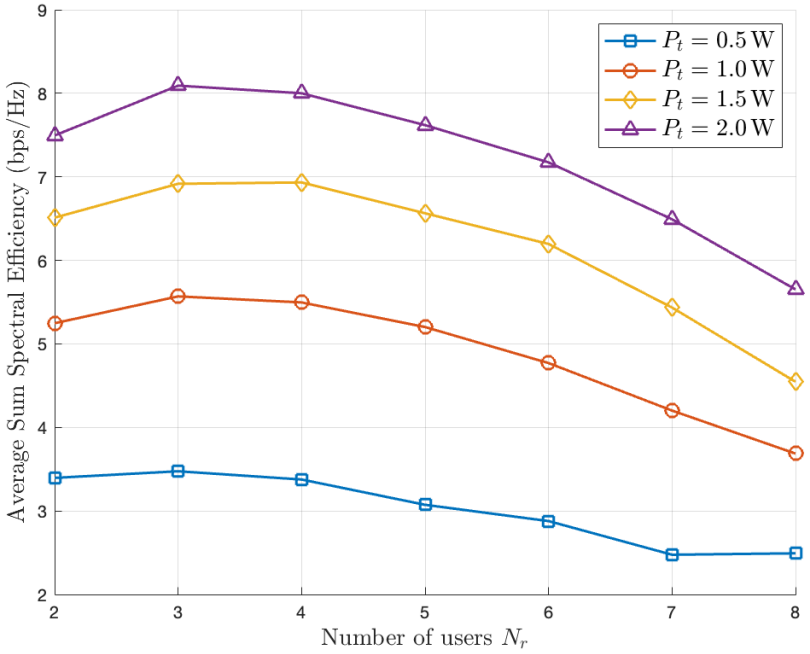

Figure 5.2: Sum spectral efficiency of 1-RSMA versus number of users N_r for four optical transmit-power budgets.

under the same power reduces the SE by ~33%, underlining the importance of user-load control in dense VLC deployments.

To elucidate how 1-RSMA balances the common and private streams under different user loads, Figure 5.3 reports the individual rates as the transmit power grows from 35 dBm to 65 dBm for (a) a light load ($N_r = 3$) and (b) a dense load ($N_r = 7$). For $N_r = 3$ the private rates of all users increase almost linearly with P_t, while the common rate remains at ≈ 1 bit/s/Hz and plateaus once the per-LED current ceiling is approached.

When the load rises to $N_r = 7$ the optimizer suppresses the common stream to a negligible level (<0.1 bit/s/Hz) and allocates power heterogeneously across users; the strongest user (U_7) secures up to 5.3 bit/s/Hz at moderate powers, whereas weaker users hover around 1–2 bit/s/Hz. This shift reflects the well-known RSMA operating principle: under heavy inter-user interference the common layer carries only the minimum rate needed for successive interference cancellation, and the bulk of the throughput is delivered through user-specific private streams.

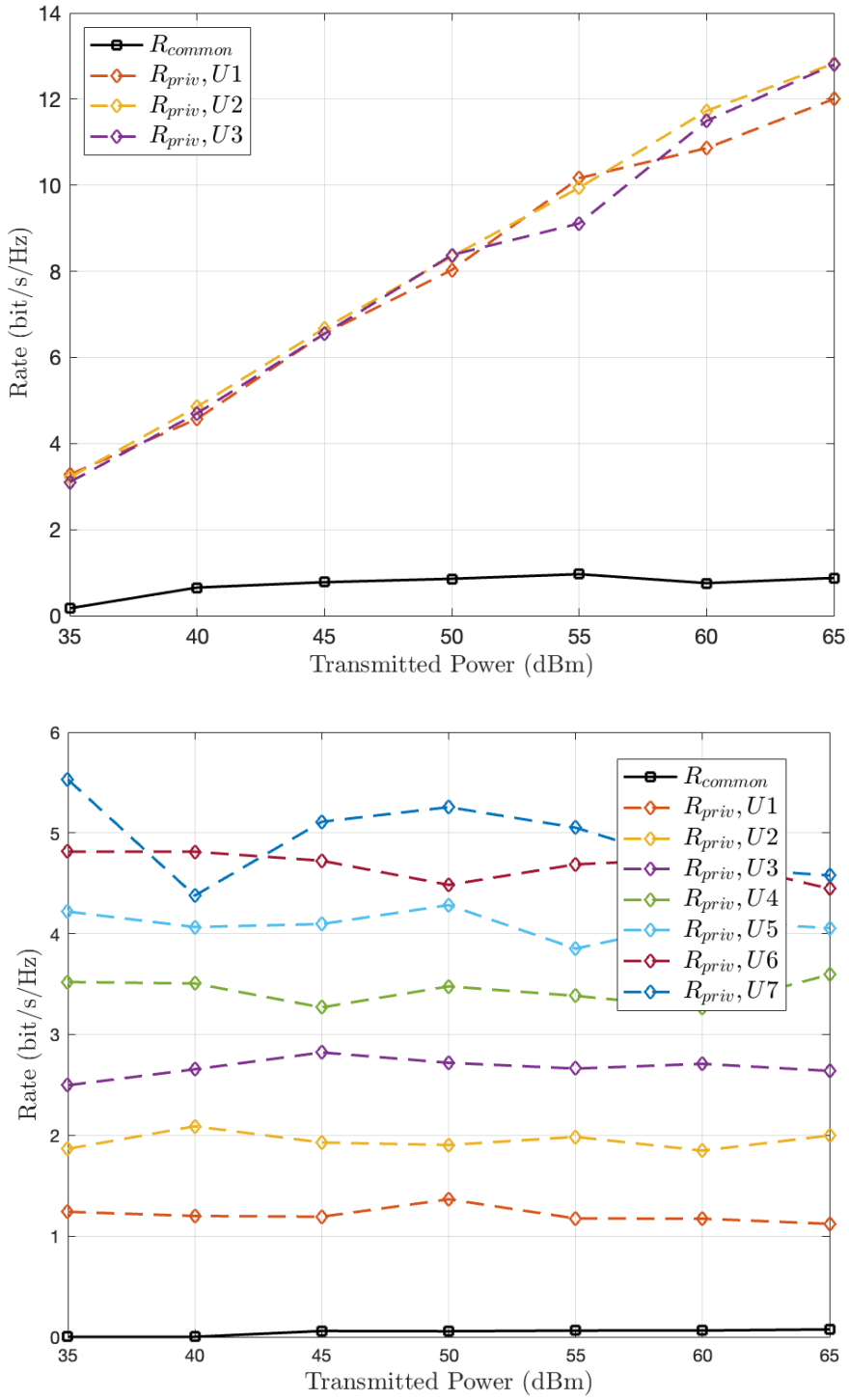

Figure 5.3: Rate decomposition of 1-RSMA: common rate $\boldsymbol{R}_{\mathrm{c}}$ and private rates $\boldsymbol{R}_{\mathrm{priv},\boldsymbol{U}_i}$ versus transmit power $\boldsymbol{P}_t$ for (a) three-user and (b) seven-user random deployments.

Figure 5.4 illustrates how the optimizer divides the per-LED transmit power among the common stream and the two private streams for a two-user deployment ($N_r = 2$) as the total power budget P_t grows from 35 dBm to 65 dBm.

Across the lower–to–mid power range (35–55 dBm) the common layer absorbs only about 15% of the modulation power, while the private layers together receive the remaining 85%, split roughly 45% / 40% between Streams 1 and 2. When P_t reaches 65 dBm the optimizer enlarges the common-stream share to about 20%, compensating for the diminishing SINR gains of the private layers, which have approached the per-LED modulation amplitude ceiling. This re-allocation maintains a balanced throughput growth: the common stream delivers interference mitigation, whereas the private streams continue to carry user-specific information without violating the current limit I_{lim}.

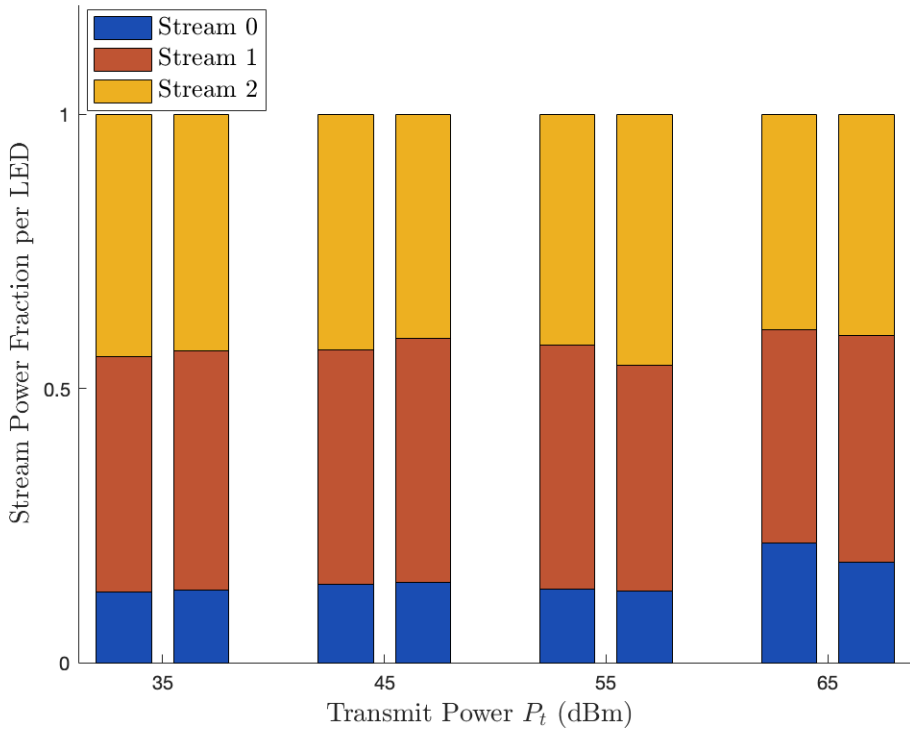

Figure 5.4: Per-LED power-allocation fractions among the common stream and two private streams versus total transmit power $\boldsymbol{P_t}$ for ($\boldsymbol{N_r = 2}$).

Figure 5.5 investigates how the spectral efficiency reacts to variations in the LED half-power semi-angle $\Phi_{1/2}$ and the PD field-of-view Ψ_{FOV}. Five practical pairs $(\Phi_{1/2}, \Psi_{\mathrm{FOV}})$ are compared while the transmit power P_t ranges from 30 dBm to 50 dBm.

The baseline optics $\Phi_{1/2} = 60°$, $\Psi_{\mathrm{FOV}} = 60°$ (blue curve) yields the highest throughput, 25 bps/Hz at $P_t = 50$ dBm, because its narrow beam and receiver aperture maximize the LOS channel gain. Increasing either angle reduces the optical directivity and thus attenuates the channel gain, leading to a nearly parallel but downward-shifted SE curve; for example, the wide-aperture setting $\Phi_{1/2} = 80°$, $\Psi_{\mathrm{FOV}} = 80°$ (green curve) achieves only 22 bps/Hz at 50 dBm.

The roughly constant vertical gap between curves indicates that optical front-end parameters act as a multiplicative channel-gain factor rather than altering the SINR slope with respect to P_t. Hence, careful joint selection of $\Phi_{1/2}$ and Ψ_{FOV} offers a straightforward means to trade off coverage versus peak throughput in RSMA-based VLC systems.

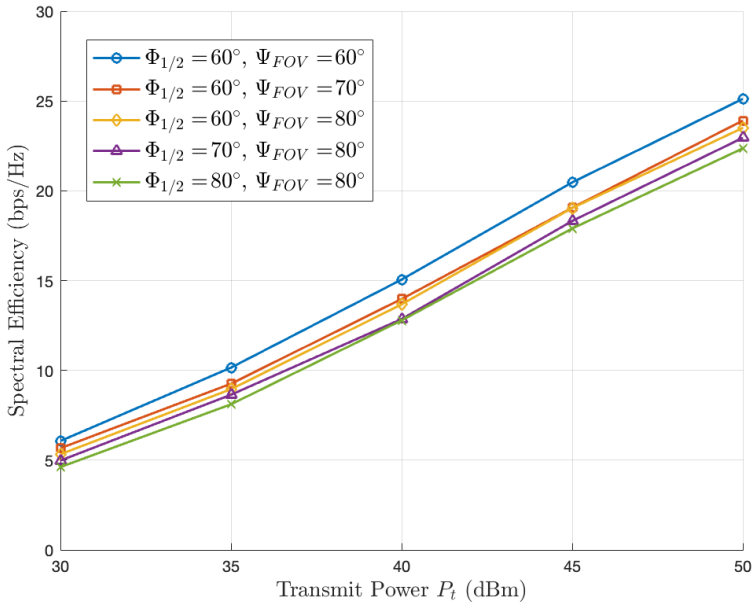

Figure 5.5: Sum spectral efficiency versus transmit power $\boldsymbol{P_t}$ with varies $\boldsymbol{\Phi_{1/2}}$ and $\boldsymbol{\Psi_{\mathrm{FOV}}}$, when $\boldsymbol{N_r = 2}$.

5.2 RESULTS FROM CONFIGURATION 2

Configuration 2 evaluates the spatial robustness of 1-RSMA by fixing one user at a pre-determined location while sweeping the second user over the room grid. In all simulations, the baseline parameters in Table 4.1 were adopted, with the total optical power set to $P_t = 50dBm$. Similar to *Configuration 1*, performance is estimated via a Monte-Carlo procedure; however, with only 10 Monte-Carlo realizations. Because the SE surface is evaluated at every cell of a fine $25cm \times 25cm$ grid, (see: Section 4.3, Figure 4.2), the increased spatial sampling provides broad statistical smoothing, allowing a reduced Monte-Carlo count without compromising reliability while significantly shortening runtime.

As discussed in Section4.3, three representative user deployment scenarios are considered.

Scenario i: The fixed user is near the room edge.
Scenario ii: The fixed user is directly below the first LED.
Scenario iii: The fixed user is centered between the two LEDs.

The coordinates (*x, y, z*) of the fixed user for each scenario are summarized in Table 5.1.

Table 5.1: Fixed-user coordinates for the three spatial-sweep scenarios in Configuration 2.

Scenario	Fixed User Position (x, y, z) (m)
i	0.5, 0.5, 1.0
ii	7.5, 3.5, 1.0
iii	4.5, 2.0, 1.0

Figure 5.6 visualizes the spatial distribution of the sum SE when a second user is swept across the room grid while the first user remains at the fixed coordinates listed in Table 5.1.

In *Scenario i* the SE surface is dominated by LED 2; the vertical color discontinuity along $x \approx 5$ m reflects the hand-over line where the strongest LOS channel switches from LED 1 to LED 2.

In *Scenario ii* the high-throughput region shrinks towards the north-west quarter, and performance degrades rapidly once the swept user approaches the opposite corner, a manifestation of path-loss imbalance and intensified inter-user interference.

Scenario iii, with the fixed user centered between the two LEDs, exhibits the most balanced landscape: peak SE values appear around both luminaries, while the valley along the diagonal seam is less pronounced, confirming that symmetric user placement alleviates channel disparity and enables more efficient power splitting.

Figure 5.7 contrasts the per-LED power split among the common stream and the two private streams for the three fixed-user deployments of Configuration 2. Across all cases the common layer absorbs only 8–15 % of the modulation budget, confirming that 1-RSMA relies primarily on the private layers when the user load is low. The private-stream fractions, however, vary markedly with geometry.

In *Scenario i*, the optimizer dedicates roughly 60% of the power to the stream serving that edge user, while the center-room stream receives 30–35%. When the fixed user sits directly below LED 1 *Scenario ii* the power share shifts further toward that user (≈70 \%), reflecting its weaker link to LED 2 and the need to compensate for the path-loss imbalance. In contrast, the symmetric placement in *Scenario iii* yields a more balanced split (≈45% vs. 40%), illustrating that geometric symmetry mitigates stream-power asymmetry and improves fairness without sacrificing total performance.

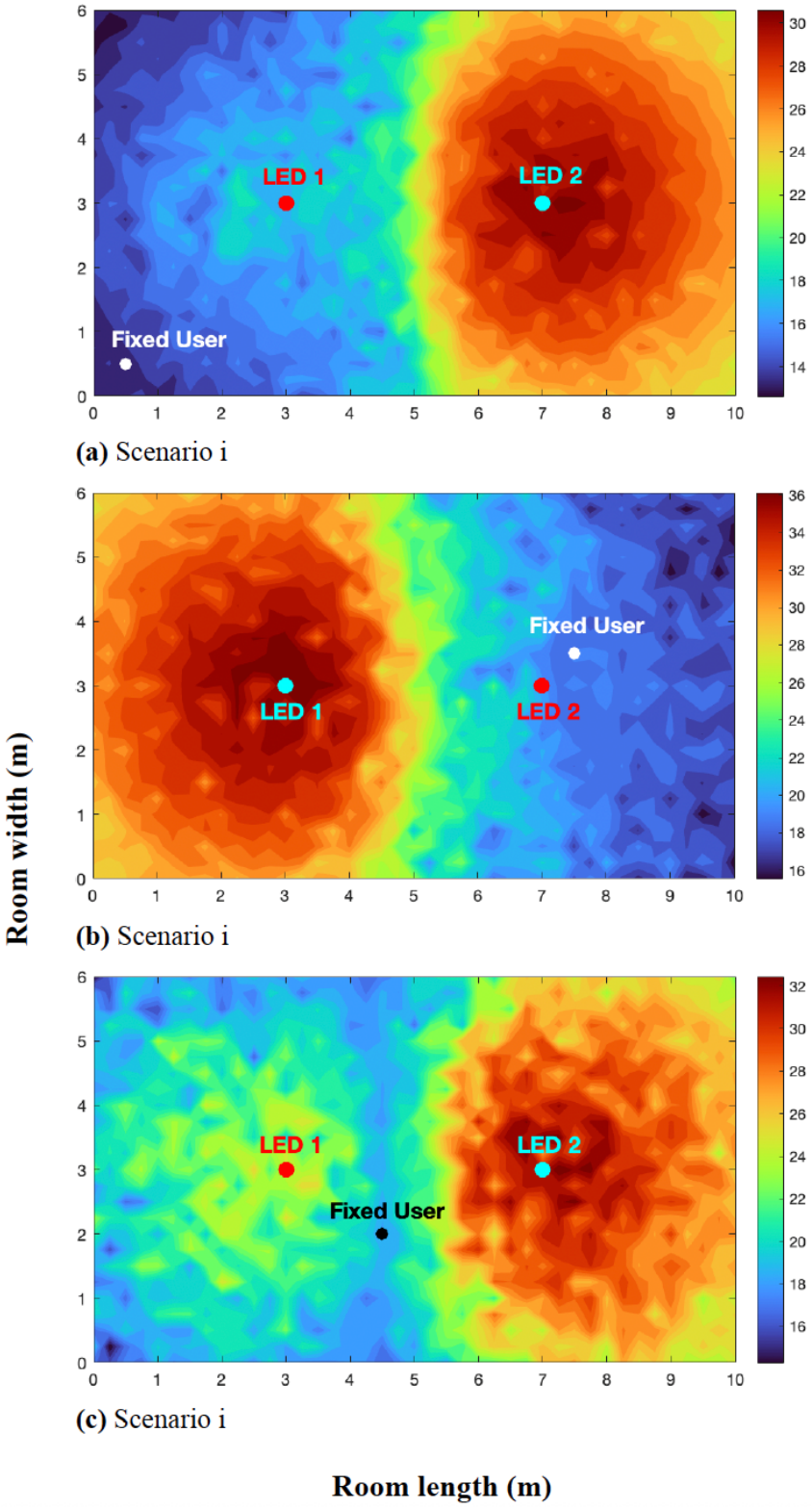

Figure 5.6: Spatial RSMA spectral-efficiency maps for the three scenarios.

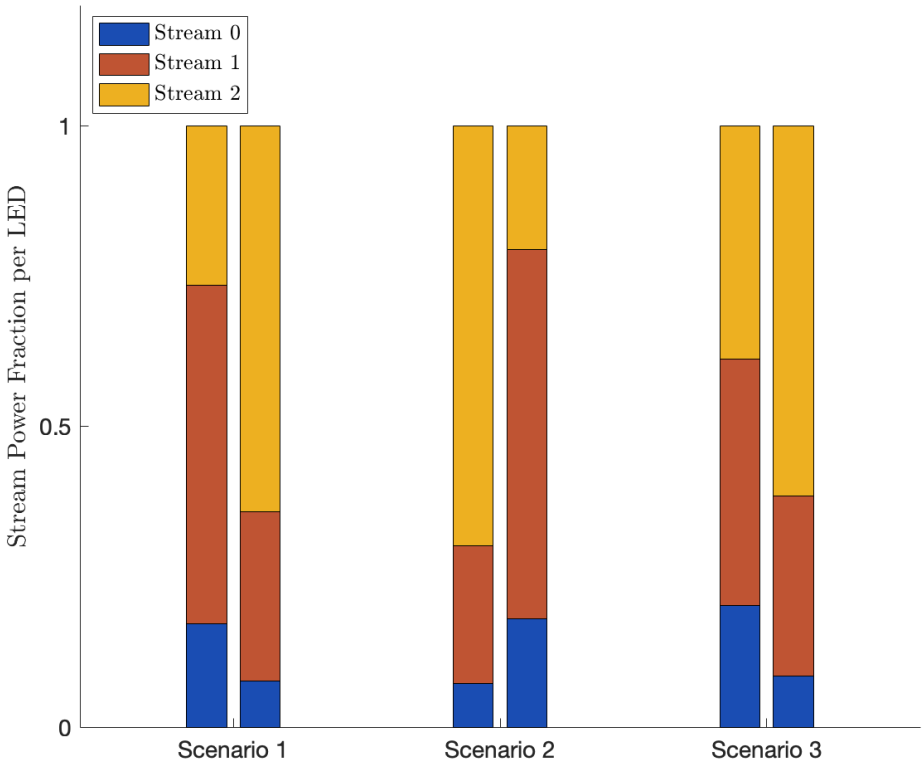

Figure 5.7: Per-LED modulation-power fractions allocated to the common stream and the two private streams for the three scenarios in Configuration 2.

5.3 DISCUSSION

This chapter has systematically investigated the performance of 1-RSMA in indoor VLC environments through comprehensive numerical evaluations. The analysis encompassed a range of scenarios, system conditions, and hardware constraints, providing a thorough exploration of RSMA's capabilities and practical deployment.

The previous results show how 1-RSMA performs when we change four key factors: (i) total transmit power, (ii) number of users, (iii) users' positions in the room, and (iv) optical parameters. In this section we bring these findings together.

5.3.1 Power–Scaling Behavior

Figure 5.1 demonstrates that 1-RSMA consistently outperforms PD-NOMA throughout the entire 35−65 dBm transmit-power range and for every user load examined.

At the lower power budget of 35 dBm, the relative SE gain of RSMA is already significant: about 50% for two users, increasing to roughly 111% for three users, 280% for five users, and 300% for seven users. These large percentages arise because, under tight current constraints, RSMA can concentrate most of the modulation swing on the two private streams while still conveying a small common stream, whereas NOMA suffers from severe power dilution across users.

Raising the optical budget to 65 dBm increases the absolute gains while moderating the relative ones: RSMA delivers approximately 37 bps/Hz versus 26 bps/Hz for NOMA at $N_r = 2$ (a 42% improvement) and 40 bps/Hz versus 24.5 bps/Hz at $N_r = 3$ (a 63% improvement). For heavier loads the relative advantage remains substantial, around 46% for $N_r = 5$ and 80% for N_r =7, corresponding to absolute increases of 12.5 bps/Hz and 16.5 bps/Hz, respectively.

The curves flatten beyond roughly 60 dBm, forming the shallow "dome'' in Figure 5.1. This knee coincides with the per-LED current ceiling I_{lim}; once any LED reaches its linearity limit, additional optical power is absorbed almost entirely by the DC bias and no longer enhances the usable signal. Further throughput growth would therefore require either adding more emitters or relaxing driver-current constraints.

In summary, RSMA provides modest yet meaningful gains at light loads and delivers dramatic improvements, both absolute and relative, under realistic high-density VLC conditions, clearly validating its adoption for next-generation indoor optical wireless systems.

5.3.2 User-Load Dynamics

Varying the number of active users produces a peak at $N_r \approx 3-4$ for all power budgets (Figure 5.2). The initial rise benefits from multi-user diversity, whereas the subsequent decline is dominated by two factors: (i) *power dilution* across a larger set of private streams and (ii) *residual interference* that grows with user density. The rate decomposition curves in Figure 5.3 confirm that, at low loads, the common layer carries ≤ 1 bit/s/Hz and the private layers scale almost linearly with P_t. When the network becomes overloaded ($N_r = 7$), the optimizer essentially suppresses the common stream and allocates power into the two strongest users, sacrificing fairness to preserve aggregate SE. This strategy maximizes the total spectral efficiency but does so at the cost of rate balance among users, illustrating the classic throughput–fairness trade-off inherent in power-limited RSMA systems.

5.3.3 Spatial Heterogeneity

The heat-maps in Figure 5.6 make clear that user geometry alone can shift both the level and uniformity of SE. When the fixed user is in a room corner (Scenario i), the SE surface is highly asymmetric and the optimizer pours most of the power into the private stream of the user on the edge. Fixing the user directly under a luminary (Scenario ii) yields even steeper gains and losses as the swept user moves, further skewing the power split (Figure 5.7). In contrast, placing the fixed user midway between the two LEDs (Scenario iii) flattens the SE landscape and produces a near-symmetric power allocation. In short, corner or under-LED placements maximize local peaks, whereas a mid-room anchor delivers smoother coverage and fairer power sharing, underscoring geometry as a first-order design variable in RSMA-VLC systems.

5.3.4 Optical Parameters

Altering the LED $\Phi_{1/2}$ or the PD Ψ_{FOV} shifts every SE vs. P_t curve by an almost constant offset (Figure 5.5). This behavior confirms that *optics act as a multiplicative channel-gain factor*: tighter beams or narrower FOVs linearly amplify the DC channel gain but do not change the SINR or rate slope. Designers can therefore treat $\Phi_{1/2}$ and Ψ_{FOV} as knobs: narrowing them boosts SE, while widening them does the opposite, without requiring any changes to the 1-RSMA routine.

Altogether, the outcomes presented in this chapter validate the advantages of RSMA as a robust, flexible, and highly effective multiple-access solution in VLC systems. The adaptability of RSMA to a variety of user geometries, system constraints, and operational scenarios positions it as a versatile framework suitable for diverse indoor communication environments. Future efforts should focus on extending these findings to address real-world channel impairments, multi-cell interference, and dynamic conditions, further cementing RSMA's role in next-generation optical wireless communications.

5.4 FUTURE WORK

While the current study demonstrates the viability and advantages of RSMA in downlink VLC systems under idealized conditions, several avenues remain open for future exploration to enhance the realism, and system-level impact of the proposed framework.

Future extensions of this study should begin by relaxing the perfect-CSIT assumption and introducing robust optimization techniques that account for channel estimation errors, quantized feedback, and outdated CSI. By formulating bounded-error or stochastic RSMA precoding and power-allocation problems, one can quantify the scheme's resilience relative to PD-NOMA in the face of realistic CSI uncertainty. In parallel, the room-scale spatial-sweep methodology can be adapted to dynamic scenarios: modeling user mobility along

predefined trajectories or intermittent blockage by obstacles (e.g. furniture or human bodies) will enable the development of low-latency stream reallocation heuristics that track time-varying LOS conditions.

Another valuable modeling step is to move beyond the pure LOS Lambertian channel and incorporate first-order reflections and diffuse scattering via Monte Carlo ray tracing. Such an analysis would reveal how NLOS components affect RSMA's interference-mitigation benefits and could guide the placement of reflective surfaces in indoor environments. On the experimental side, prototyping a MISO system, including nonlinearity of the LED driver and DC bias constraints, would allow direct observation of the SE 'knee' and dome phenomena, validating simulation predictions. Finally, extending the performance metric to include energy efficiency by jointly optimizing SE and power consumption will clarify the throughput–energy trade-offs and inform the design of sustainable and high-performance VLC access points.

Finally, the integration of machine learning techniques, particularly reinforcement learning and deep neural networks, offers a promising pathway toward real-time adaptation and complexity reduction. Traditional optimization approaches, while powerful, are often computationally intensive and unsuitable for low-latency VLC applications involving user mobility, dynamic traffic patterns, or time-varying constraints. ML-based frameworks could be trained to approximate the RSMA precoding and power allocation policies in an online or semi-supervised manner, enabling fast and adaptive decision-making without the need for full re-optimization. Furthermore, offline-trained models could leverage historical deployment data to generalize across environments, user topologies, or hardware profiles. The separation of direction and amplitude in the RSMA model, as discussed in this thesis, aligns well with structured learning paradigms that allow hybrid policy spaces, combining discrete direction choices with continuous power amplitudes, thus reducing the learning burden, and enabling more interpretable model behaviors.

CONCLUSION & SUGGESTIONS

This thesis has investigated the applicability and performance benefits of one-layer Rate-Splitting Multiple Access (1-RSMA) in downlink indoor Visible Light Communication (VLC) systems under realistic operational constraints. By incorporating practical Lambertian line-of-sight (LOS) channel modeling, LED current linearity constraints, and user-centric power allocation strategies, this research provides novel insights into the capabilities and limitations of RSMA as an advanced multiple access technique in optical wireless communications.

Through extensive Monte Carlo simulations and spatial sensitivity analyses, RSMA consistently demonstrated superior spectral efficiency (SE) performance compared to power-domain Non-Orthogonal Multiple Access (PD-NOMA). RSMA achieved significant SE gains compared to PD-NOMA across all user densities and power budgets. At the lower power budget of 35~dBm, the relative spectral efficiency gain of RSMA was about 50% for two users, increasing to roughly 111% for three users, 280% for five users, and 300% for seven users. At the higher power budget of 65 dBm, the gains remained substantial, with improvements of 42% for two users, 63% for three users, 46% for five users, and 80% for seven users. These results confirm that RSMA's advantage is particularly pronounced at low-to-moderate power levels and higher user densities, due to its ability to flexibly allocate power and manage multi-user interference.

The performance evaluations highlighted four key influences on RSMA efficacy: optical transmit power, user load, spatial distribution, and optical hardware parameters. Increasing transmit power exhibited diminishing returns beyond certain thresholds due to LED hardware constraints, emphasizing the importance of optimized LED operation points and power allocation. Furthermore, user density analyses revealed a clear trade-off between spectral efficiency and fairness, particularly at higher loads where prioritizing strong user channels maximized aggregate SE at the expense of balanced throughput

distribution.

Spatial sensitivity analyses illustrated the significant impact of user placement on RSMA performance. Corner and central room placements displayed distinct power allocation profiles and SE distributions, underscoring the necessity of careful planning of luminaire and receiver geometries to maximize overall throughput and ensure consistent service coverage. Additionally, adjustments in optical front-end parameters such as the LED semi-angle ($\Phi_{1/2}$) and PD field-of-view (Ψ_{FOV}) offered direct control over SE performance, highlighting their importance in practical VLC system design.

Future research directions should prioritize the incorporation of realistic channel uncertainties, robust precoding methods, and adaptive resource management for dynamic user scenarios, such as mobility and blockage. Investigations should also consider non-LOS and multi-path propagation through ray-tracing models to enhance realism. Experimental validation of RSMA-based MISO-VLC systems is necessary to confirm theoretical and numerical findings while exploring practical hardware limitations. Jointly optimizing spectral and energy efficiency will further support sustainable VLC deployment. Finally, machine learning methods, including reinforcement learning and deep neural networks, hold potential for reducing computational complexity and facilitating real-time adaptive resource allocation.

Addressing these fields will significantly enhance the practical applicability, scalability, and efficiency of RSMA-based VLC deployments, paving the way toward advanced optical wireless communication solutions. Overall, this work demonstrates the viability of RSMA to push VLC spectral efficiencies beyond what PD-NOMA can achieve under real-world constraints, laying a solid foundation for next-generation optical wireless networks.

REFERENCES

Chaaban, A., Morvan, J.-M., & Alouini, M.-S. (2016). Free-Space Optical Communications: Capacity Bounds, Approximations, and a New Sphere-Packing Perspective. *IEEE Transactions on Communications*, *64*(3), 1176–1191. https://doi.org/10.1109/TCOMM.2016.2524569

Cisco. (2019). Cisco global cloud index: Forecast and methodology, 2016–2021. *White Paper*.

Girdher, A., Gupta, N., & Bansal, A. (2024). Fairness-Aware Energy Harvesting in RSMA-Aided MU-MISO VLC Network. *IEEE Communications Letters*, *28*(5), 1062–1066. https://doi.org/10.1109/LCOMM.2024.3380418

Guo, Y., Fan, J., Zhang, R., Chang, B., Ng, D. W. K., Niyato, D., & Kim, D. I. (2025). Secrecy Energy Efficiency Maximization in IRS-Assisted VLC MISO Networks with RSMA: A DS-PPO Approach. *IEEE Transactions on Wireless Communications*, 1–1. https://doi.org/10.1109/TWC.2025.3553843

Guo, Y., Xiong, K., Gao, B., Fan, P., Ng, D. W. K., & Letaief, K. B. (2024). Max–Min Fairness in Rate-Splitting Multiple-Access-Based VLC Networks With SLIPT. *IEEE Internet of Things Journal*, *11*(22), 36508–36520. https://doi.org/10.1109/JIOT.2024.3412430

Hu, J., Sun, C., Wang, J., Gao, X., Xia, L., & Wang, Q. (2024). Resource Efficient and Robust RSMA for Visible Light Communications. *IEEE Photonics Journal*, *16*(4), 1–12. https://doi.org/10.1109/JPHOT.2024.3388472

Hu, J., Sun, C., Wang, J., Gao, X., & Zhao, C. (2023). Common Rate Allocation and Power Control Optimization for RSMA-Based Visible Light Communications. *2023 IEEE 97th Vehicular Technology Conference (VTC2023-Spring)*, 1–6. https://doi.org/10.1109/VTC2023-Spring57618.2023.10200448

Jiang, R., Wang, Q., Haas, H., & Wang, Z. (2018). Joint User Association and Power Allocation for Cell-Free Visible Light Communication Networks. *IEEE Journal on Selected Areas in Communications*, *36*(1), 136–148. https://doi.org/10.1109/JSAC.2017.2774400

Jovicic, A., Li, J., & Richardson, T. (2013). Visible light communication: Opportunities, challenges and the path to market. *IEEE Communications Magazine*, *51*(12), 26–32.

https://doi.org/10.1109/MCOM.2013.6685754

Kowshik, A. K., Gurugopinath, S., & Muhaidat, S. (2024). ViRSMALNet: A Twin-Tier LSTM-Based Deep Learning Network for Indoor MIMO RSMA VLC Systems. *IEEE Open Journal of the Communications Society*, *5*, 2735–2747. https://doi.org/10.1109/OJCOMS.2023.3336772

Lapidoth, A., Moser, S. M., & Wigger, M. A. (2009). On the Capacity of Free-Space Optical Intensity Channels. *IEEE Transactions on Information Theory*, *55*(10), 4449–4461. https://doi.org/10.1109/TIT.2009.2027522

Liu, Q., Xie, X., Wang, X., Wang, W., & Lu, L. (2023). Rate Splitting Multiple Access Enhanced Visible Light Communications under Fairness Constraint. *2023 9th International Conference on Computer and Communications (ICCC)*, 125–130. https://doi.org/10.1109/ICCC59590.2023.10507342

Lucas, J. (2022). What is visible light? In *LiveScience*. Purch. https://www.livescience.com/50678-visible-light.html

Ma, S., Zhang, G., Zhang, Z., Gu, R., Wu, Y., & Li, S. (2022). Rate Splitting Multiple Access-Aided MISO Visible Light Communications. *2022 International Symposium on Wireless Communication Systems (ISWCS)*, 1–6. https://doi.org/10.1109/ISWCS56560.2022.9940414

Mao, Y., Clerckx, B., & Li, V. O. K. (2018). Rate-splitting multiple access for downlink communication systems: Bridging, generalizing, and outperforming SDMA and NOMA. *EURASIP Journal on Wireless Communications and Networking*, *2018*(1). https://doi.org/10.1186/s13638-018-1104-7

Mao, Y., Dizdar, O., Clerckx, B., Schober, R., Popovski, P., & Poor, H. V. (2022). Rate-Splitting Multiple Access: Fundamentals, Survey, and Future Research Trends. *IEEE Communications Surveys & Tutorials*, *24*(4), 2073–2126. https://doi.org/10.1109/COMST.2022.3191937

Maraqa, O., Aboagye, S., Khoshafa, M. H., & Ngatched, T. M. N. (2025). Max-Min Secrecy Rate and Secrecy Energy Efficiency Optimization for RIS-Aided VLC Systems: RSMA Versus NOMA. *IEEE Open Journal of Vehicular Technology*, 1–14. https://doi.org/10.1109/OJVT.2025.3568436

Maraqa, O., Aboagye, S., & Ngatched, T. M. N. (2024). Optical STAR-RIS-Aided VLC Systems: RSMA Versus NOMA. *IEEE Open Journal of the Communications Society*, *5*, 430–441. https://doi.org/10.1109/OJCOMS.2023.3347534

Marshoud, H., Kapinas, V. M., Karagiannidis, G. K., & Muhaidat, S. (2016). Non-Orthogonal Multiple Access for Visible Light Communications. *IEEE Photonics Technology Letters*, *28*(1), 51–54. https://doi.org/10.1109/LPT.2015.2479600

Marshoud, H., Muhaidat, S., Sofotasios, P. C., Hussain, S., Imran, M. A., & Sharif, B. S. (2018). Optical Non-Orthogonal Multiple Access for Visible Light Communication. *IEEE Wireless Communications*, *25*(2), 82–88. https://doi.org/10.1109/MWC.2018.1700122

Miramirkhani, F., & Uysal, M. (2015). Channel Modeling and Characterization for Visible Light Communications. *IEEE Photonics Journal*, *7*(6), 1–16. https://doi.org/10.1109/JPHOT.2015.2504238

Mohsan, S. A. H., Sadiq, M., Li, Y., Shvetsov, A. V., Shvetsova, S. V., & Shafiq, M. (2023). NOMA-Based VLC Systems: A Comprehensive Review. *Sensors*, *23*(6). https://doi.org/10.3390/s23062960

Naser, S. A., Sofotasios, P. C., Muhaidat, S., & Al-Qutayri, M. (2021). Rate-Splitting Multiple Access for Indoor Visible Light Communication Networks. *2021 IEEE Wireless Communications and Networking Conference Workshops (WCNCW)*, 1–7. https://doi.org/10.1109/WCNCW49093.2021.9419979

Naser, S., Bariah, L., Jaafar, W., Muhaidat, S., Al-Qutayri, M., Uysal, M., & Sofotasios, P. C. (2022). Coordinated Beamforming Design for Multi-User Multi-Cell MIMO VLC Networks. *IEEE Photonics Journal*, *14*(3), 1–10. https://doi.org/10.1109/JPHOT.2022.3169233

Naser, S., Sofotasios, P. C., Bariah, L., Jaafar, W., Muhaidat, S., Al-Qutayri, M., & Dobre, O. A. (2020). Rate-Splitting Multiple Access: Unifying NOMA and SDMA in MISO VLC Channels. *IEEE Open Journal of Vehicular Technology*, *1*, 393–413. https://doi.org/10.1109/OJVT.2020.3031656

Nguyen, T. K., Pham, T. V., Nguyen, C. T., & Pham, A. T. (2024). On the Energy Efficiency of RSMA-Based VLC Systems with Confidential Private Messages. *2024 IEEE Wireless Communications and Networking Conference (WCNC)*, 1–6. https://doi.org/10.1109/WCNC57260.2024.10570924

Pathak, P. H., Feng, X., Hu, P., & Mohapatra, P. (2015). Visible Light Communication, Networking, and Sensing: A Survey, Potential and Challenges. *IEEE Communications Surveys & Tutorials*, *17*(4), 2047–2077. https://doi.org/10.1109/COMST.2015.2476474

Prabhakar, H., Chaturvedi, S., Gupta, A., & Bohara, V. A. (2024). Performance

Analysis of THz and VLC Systems Under the Impact of Weather and Human Blockages. *TENCON 2024 - 2024 IEEE Region 10 Conference (TENCON)*, 206–209. https://doi.org/10.1109/TENCON61640.2024.10902759

Qiu, Z., Mao, Y., Ma, S., & Clerckx, B. (2025). Robust Max–Min Fair Beamforming Design for Rate Splitting Multiple Access-Aided Visible Light Communications. *IEEE Internet of Things Journal*, *12*(8), 10043–10057. https://doi.org/10.1109/JIOT.2024.3509917

Rallis, K. G., Papanikolaou, V. K., Tegos, S. A., Dowhuszko, A. A., Diamantoulakis, P. D., Khalighi, M.-A., & Karagiannidis, G. K. (2023). RSMA Inspired User Cooperation in Hybrid VLC/RF Networks for Coverage Extension. *2023 IEEE Wireless Communications and Networking Conference (WCNC)*, 1–6. https://doi.org/10.1109/WCNC55385.2023.10118918

Salam, R., Bohara, V. A., & Srivastava, A. (2025). Smart Element Allocation Strategies for Dynamic Optical IRS in Underwater Wireless Communication. *IEEE Transactions on Vehicular Technology*, *74*(3), 4349–4361. https://doi.org/10.1109/TVT.2024.3492284

Shen, H., Deng, Y., Xu, W., & Zhao, C. (2016). Rate Maximization for Downlink Multiuser Visible Light Communications. *IEEE Access*, *4*, 6567–6573. https://doi.org/10.1109/ACCESS.2016.2614598

Shen, H., Wu, Y., Xu, W., & Zhao, C. (2017). Optimal Power Allocation for Downlink two-User Non-Orthogonal Multiple Access in Visible Light Communication. *Journal of Communications and Information Networks*, *2*(4), 57–64. https://doi.org/10.1007/s41650-017-0037-3

Soderi, S., & De Nicola, R. (2022). 6G Networks Physical Layer Security Using RGB Visible Light Communications. *IEEE Access*, *10*, 5482–5496. https://doi.org/10.1109/ACCESS.2021.3139456

Xing, F., He, S., Leung, V. C. M., & Yin, H. (2022). Energy Efficiency Optimization for Rate-Splitting Multiple Access-Based Indoor Visible Light Communication Networks. *IEEE Journal on Selected Areas in Communications*, *40*(5), 1706–1720. https://doi.org/10.1109/JSAC.2022.3145818

Zhang, R., Chen, C., Zhong, X., Liu, M., Yang, Y., & Duan, X. (2021). On the Sum Rate of Precoded Multi-User SDMA VLC System with Limited Dynamic Range. *2021 Asia Communications and Photonics Conference (ACP)*, 1–3.

Zhou, J., & Zhang, W. (2019). Bounds on the Capacity Region of the Optical

Intensity Multiple Access Channel. *IEEE Transactions on Communications*, *67*(11), 7629–7641. https://doi.org/10.1109/TCOMM.2019.2938748

CURRICULUM VITAE